Title

Stockwork-like sulfide mineralization in young oceanic crust: Deep Sea Drilling Project hole 504B.

Authors

Honnorez, J

Alt, JC

Honnorez-Guerstein, B

et al.

Publication Date

1985

DOI

10.2973/dsdp.proc.83.110.1985

10. STOCKWORK-LIKE SULFIDE MINERALIZATION IN YOUNG OCEANIC CRUST: DEEP SEA DRILLING PROJECT HOLE 504B[1]

J. Honnorez, J. C. Alt, B.-M. Honnorez-Guerstein, C. Laverne, K. Muehlenbachs, J. Ruiz, and E. Saltzman,
Rosenstiel School of Marine and Atmospheric Science, University of Miami[2]

ABSTRACT

Stockwork-like metal sulfide mineralizations were found at 910–928 m below seafloor (BSF) in the pillow/dike transition zone of Hole 504B. This is the same interval where most physical properties of the 5.9-m.y.-old crust of the Costa Rica Rift change from those characteristic of Layer 2B to those of Layer 2C. The pillow lavas, breccias, and veins of the stockwork-like zone were studied by transmitted and reflected light microscopy, X-ray diffraction, and electron microprobe analysis. Bulk rock oxygen isotopic analyses as well as isolated mineral oxygen and sulfur isotopic analyses and fluid inclusion measurements were carried out. A complex alteration history was reconstructed that includes three generations of fissures, each followed by precipitation of characteristic hydrothermal mineral parageneses: (1) Minor and local deposition of quartz occurred on fissure walls; adjacent wall rocks were silicified, followed by formation of chlorite and minor pyrite I in the veins, whereas albite, sphene, chlorite and chlorite-expandable clay mixtures, actinolite, and pyrite replaced igneous phases in the host rocks. The hydrothermal fluids responsible for this first stage were probably partially reacted seawater, and their temperatures were at least 200–250°C. (2) Fissures filled during the first stage were reopened and new cracks formed. They were filled with quartz, minor chlorite and chlorite-expandable clay mixtures, traces of epidote, common pyrite, sphalerite, chalcopyrite, and minor galena. During the second stage, hydrothermal fluids were relatively evolved metal- and Si-rich solutions whose temperatures ranged from 230 to 340°C. The fluctuating chemical composition and temperature of the solutions produced a complex depositional sequence of sulfides in the veins: chalcopyrite I, ± Fe-rich sphalerite, chalcopyrite II ("disease"), Fe-poor sphalerite, chalcopyrite III, galena, and pyrite II. (3) During the last stage, zeolites and Mg-poor calcite filled up the remaining spaces and newly formed cracks and replaced the host rock plagioclase. Analcite and stilbite were first to form in veins, possibly at temperatures below 200°C; analcite and earlier quartz were replaced by laumontite at 250°C, whereas calcite formation temperature ranged from 135 to 220°C. The last stage hydrothermal fluids were depleted in Mg and enriched in Ca and ^{18}O compared to seawater and contained a mantle carbon component.

This complex alteration history paralleling a complex mineral paragenesis can be interpreted as the result of a relatively long-term evolution of a hydrothermal system with superimposed shorter term fluctuations in solution temperature and composition. Hydrothermal activity probably began close to the axis of the Costa Rica Rift with the overall cooling of the system and multiple fracturing stages due to movement of the crust away from the axis and/or cooling of a magmatic heat source.

INTRODUCTION

Accumulations of heavy metal sulfides on the seafloor of fast spreading centers have recently attracted the attention of a large community including scientists, mining interests, and legislative and political authorities. Reserves have been valued at $2 billion for copper alone in the case of the Galapagos Spreading Center; however, this estimate appears to be premature and optimistic at best. Massive sulfide deposits have been mined, some of them since antiquity, from deposits associated with ophiolite complexes of Cyprus, the Appennines, Newfoundland, Oman, and Corsica. Indicators of such mineralizations have also been found in the Oman ophiolites. However, no mining operation is taking place now in any of the ophiolite complexes. The sulfide accumulations at fast spreading centers have been compared with the ophiolitic massive sulfide deposits and, indeed, some textural and mineralogical similarities were found (Oudin et al., 1981). As a consequence, the ocean floor sulfide accumulations have been improperly called "massive sulfide *deposits*" even though they presently have no economical value.

Disseminated iron-copper sulfide mineralizations are already known to occur in samples of metamorphosed pillow basalts dredged from the equatorial Mid-Atlantic Ridge fracture zones (Bonatti et al., 1976) where they occur in veins with metamorphic silicates characteristic of the greenschist and zeolite facies.

Heavy metal sulfide mineralizations were encountered in a network of veinlets cutting pillow basalts and pillow breccias in two successive cores recovered from the pillow/dike transition zone of Hole 504B. The gangue accompanying the metallic sulfides both in the wall rocks and the veins is made up mainly of metamorphic silicates belonging to mineral parageneses of both the zeolite and greenschist facies.

The purpose of this chapter is to describe the stockwork-like[3] mineralizations found in Hole 504B and to

[1] Anderson, R. N., Honnorez, J., Becker, K., et al., *Init. Repts. DSDP*, 83: Washington (U.S. Govt. Printing Office).

[2] Addresses: (J. Honnorez, B.-M. Honnorez-Guerstein, Saltzman) Department of Marine Geology and Geophysics, Rosenstiel School of Marine and Atmospheric Science, University of Miami, Miami FL 33149; (Alt, present address) Department of Earth and Planetary Sciences, Washington University, Campus Box 1169, St. Louis, MO 63130; (Laverne) Laboratoire de Géologie, Faculté des Sciences et Techniques BPW, 3038 SFAX, Tunisia; (Muehlenbachs) Department of Geology, University of Alberta, Edmonton, Alberta, Canada T6G 2E3; (Ruiz, present address) Department of Geosciences, University of Arizona, Tucson, AZ 85721.

[3] A stockwork is defined as "a mineral deposit (i.e., usually of economic value) in the form of a network of veinlets diffused in the country rock" (Gary et al., 1974). The expression "stockwork-like" is used in this chapter in reference to the sulfide mineralizations of Hole 504B, Cores 80 and 81, as a descriptive term without implication of economic value.

suggest a sequence of hydrothermal events that occurred in the oceanic crust of the Costa Rica Rift.

DSDP HOLE 504B

Site 504 is located 200 km south of the Costa Rica Rift, the easternmost segment of the Galapagos Spreading Center (see Fig. 1). Hole 504B is situated within Magnetic Anomaly 3, with an estimated age of 5.9 m.y. The water depth is 3460 m, and the borehole penetrated a 1350-m-long section into the oceanic crust that is composed of 274.5 m of pelagic sediments and 1075.5 m of mid-ocean ridge basalt (MORB) basement.

The sediment cover is particularly thick for such a young age because the crust generated at the Costa Rica Rift moves through the equatorial high productivity zone. The sediment near the contact with basement is late Pliocene and is partly indurated to chert and limestone.

The temperature at the sediment/basement interface was measured as 59°C, whereas at the bottom of the hole it was calculated to be 165°C in the absence of disturbance resulting from drilling. The thick sediment cover has probably formed an effectively impermeable seal, preventing convective heat loss from the crust. A conductive equilibrium gradient of 190–200 mWm^{-2} was calculated from temperature measurements in the basement; this is in complete agreement with the heat flow measured at the seafloor during the site survey (Becker et al., this volume; Hobart et al., this volume).

Three major lithostratigraphic formations below the sediments were cored (see Fig. 2, Alt et al., this volume) from top to bottom: (1) 571.5 m of interlayered pillow basalts, breccias, and massive flows; (2) a 209-m-thick transition zone between the overlying extrusives and underlying intrusives; and (3) 295 m of doleritic dikes and massive units.

One of the remarkable findings resulting from the shipboard and shore-based chemical analyses is the relative uniformity of the chemical composition of the basalts from Hole 504B. Independent of their petrography or lithology, the vast majority of the basalts have a rather unevolved MORB character with high MgO and low K_2O contents and a marked large ion lithophile (LIL) depletion. Only three cooling units a few meters thick differ significantly by having higher TiO_2 contents (1.2–1.6%), high P_2O_5 contents (0.14–0.20%), and being enriched in LIL elements (Emmermann, this volume). Superimposed on the relatively uniform composition of the basaltic section are the effects of several successive alteration processes.

The stratigraphic section can be divided into three different zones on the basis of the distribution of secondary minerals with depth (Fig. 2). The pillow section (274.5–846 m below seafloor [BSF]) contains upper and lower alteration zones, which are the result of various superimposed "low-temperature" (i.e., 60–110°C) alter-

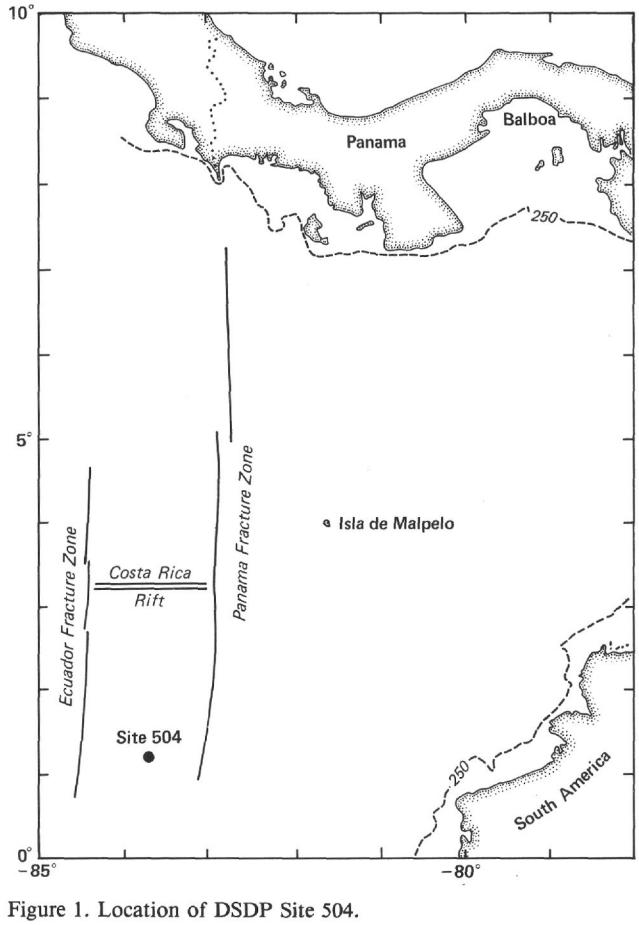

Figure 1. Location of DSDP Site 504.

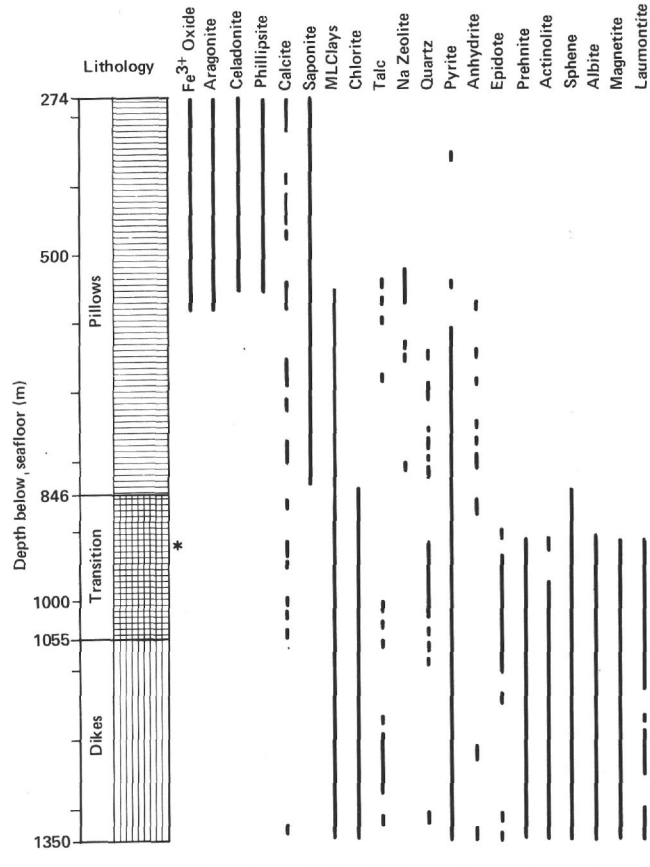

Figure 2. Lithostratigraphy and distribution of secondary minerals with depth in Hole 504B. From Alt et al., this volume. Asterisk indicates location of stockwork-like mineralization. "ML clays" indicates chlorite–expandable clay mixtures.

ation processes (Honnorez et al., 1983). The transition zone and dike sections (below 898 m BSF) are generally characterized by superimposed greenschist and zeolite facies mineral parageneses (Atl et al., this volume). Note that sphene appears and clay minerals become more chloritic at 836 m, about 74 m above the top of the stockwork zone. Thus, a gradation exists from greenschist- and zeolite-facies mineralogies in the transition zone and dikes to "low-temperature" phases in the overlying pillow section, possibly due to a steep temperature gradient (Alt et al., this volume).

The stockwork-like mineralization occurs between 910 and 928 m BSF. This is precisely the interval of the transition zone where most of the physical properties of the crust derived from downhole measurements change from those characteristic of Layer 2B to those of Layer 2C (Anderson, Honnorez, et al., 1982). The gradients of seismic velocities, density, and electrical resistivity increase, whereas the porosity gradient decreases. The cross-correlation of hydrogen-ion-sensitive neutron porosity log with porosity-sensitive γ-ray density indicates that a maximum in the abundance of secondary minerals in the rocks is reached between 910 and 930 m BSF (i.e., in the stockwork-like zone).

Bulk rocks in the stockwork-like zone exhibit increased Mn, S, H_2O, CO_2, and Na contents; decreased Si contents; and variable changes in Mg and Al relative to unaltered basalts (Alt and Emmermann, this volume; Emmermann, this volume), The variable changes in Mg contents of the Leg 83 basalts are in contrast to the general Mg enrichments that have been observed in other hydrothermally altered submarine basalts (e.g., Humphris and Thompson, 1978; Mottl, 1983) and predicted by experiments at high water/rock ratios (summary in Mottl, 1983). The Mg decreases observed in the stockwork basalts may be related in part to the density decreases observed in the rocks and the resultant net loss of material from the basalts (stockwork zone basalt densities = 2.46–2.68 versus fresh basalt densities of 2.86–3.00; Alt and Emmermann, this volume; Leg 83 shipboard reports). Samples selected for bulk rock chemical analysis were generally free of visible veins (Alt and Emmermann, this volume), but microscopic veinlets are sometimes present and may contribute slightly to the density decreases. Basalts from the stockwork also have among the lowest iron oxidation ratios in the hole (Fe^{3+}/Fe total = 0.16–0.26; Emmermann, this volume). The chemical changes in the stockwork basalts are due to the albitization and zeolitization of plagioclase, the replacement of olivine by clay minerals and pyrite, the formation of Mn-rich clay minerals and calcite, and the abundant pyrite in the basalts (Alt and Emmermann, this volume).

METHODS

Samples were studied using polished thin sections in transmitted and reflected light and by X-ray diffraction and electron microprobe. X-ray diffraction was performed using a Philips diffractometer with graphite crystal monochromator and CuKα radiation, and Debye-Scherrer and Gandolfi cameras with Mn-filtered Fe radiation. Details of clay mineral identification are given in Alt et al. (this volume). Microprobe analyses were made on the same samples identified by X-ray diffraction whenever possible. Microprobe analyses of silicates were per-

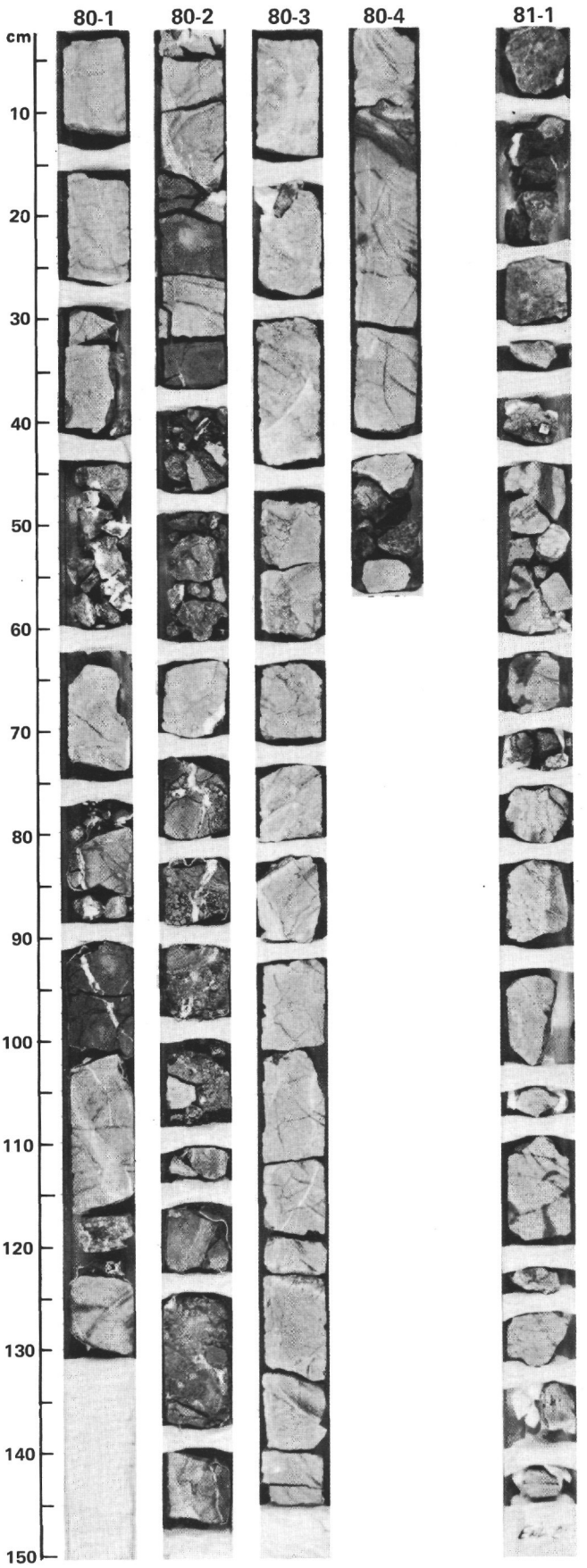

Figure 3. Photograph of the stockwork-like zone cores (Cores 504B-80 and 504B-81).

formed using a 9-channel ARL SEMQ microprobe at the Smithsonian Institution, Washington, D. C. Operating conditions were 20-KV accelerating voltage; 0.025 μA specimen current, 20 μm spot size, and 10-s counting time. Kakanui hornblende and Crystal Bay bytownite were used as standards. Computerized electron microprobe analyses of sulfides were made using the Automated Camebax instrument at the Centre Océanologique de Bretagne, Brest, France. Operating conditions were 15-KV accelerating voltage; 0.015 μA specimen current; 1 μm spot size; 6-s counting time.

MINERALOGY

Hand Specimens

The cores of the stockwork-like zone may represent either a talus pile, consisting of both small and large pillow basalt fragments, or a highly fractured pillow pile with interpillow breccias. In the following description and discussions, "basalts" refers to samples from a rock whose size is greater than the core diameter (e.g., Fig. 4), and "breccias" to samples where the rock fragments are smaller than the core diameter (e.g., Figs. 5–7).

The basalts display a light gray color, but the finer grained rocks adjacent to pillow rims are lighter in color, whereas the former glassy margins are green. Interpillow spaces are filled with pillow breccias, consisting of altered glass shards from pillow rims and holocrystalline fragments from pillow interiors cemented by dark green clay minerals (chlorite and chlorite-vermiculite mixtures). The breccias contain large (up to 2 cm long) pyrite crystal aggregates (Fig. 5). Pyrite also occurs disseminated in wall rock in thin stringers (up to 1 mm wide) sub-parallel to and up to 6 mm away from the early chlorite veins (Fig. 4). Veins of quartz, sulfides (pyrite, sphalerite, chalcopyrite, and minor galena), and rare epidote cut across or fill reopened clay mineral veins and cut across interpillow breccias (Fig. 5). These veins, in turn, are reopened and filled with or cut by veins of laumontite, heulandite, calcite, and minor analcite, stilbite, and prehnite.

Translucent Mineral Petrography

Olivine is totally replaced by chlorite-expandable clay mixtures (smectite and vermiculite; see Alt et al., this volume, for details) and pyrite (Plate 1, Fig. 4). In a few samples (e.g., Sample 504B-80-3, 124–133 cm), anhedral grains of quartz (up to 50 μm) form rims inside the perimeter of clay mineral pseudomorphs after olivine

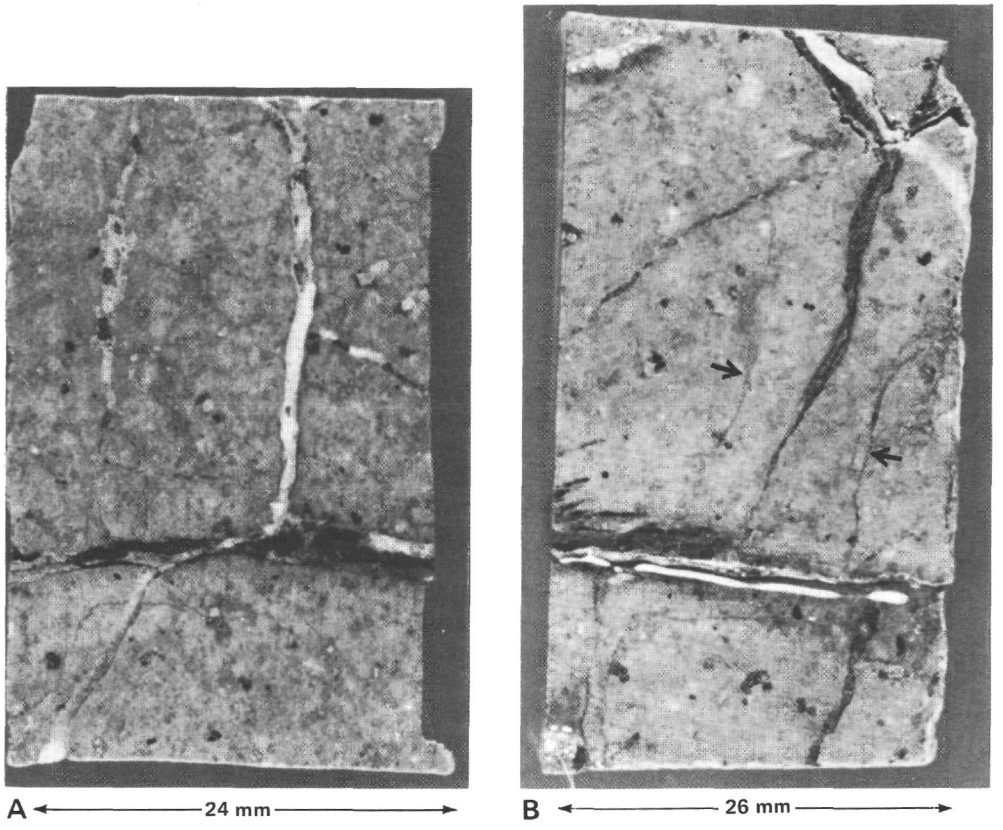

Figure 4. Sample 504B-80-1, 106–111 cm is a one-quarter section through a metamorphosed pillow interior crossed by three generations of secondary mineral veins. A and B are perpendicular cut faces on the same sample. An earlier network of Stage 1 dark green chlorite veins (black in the photograph) is accompanied by pyrite "stringers" up to 1 mm thick that run parallel to and up to 6 mm away from the chloritic veins (arrows in B). Both the chloritic veins and their pyrite stringers are intersected by later white veins (Stage 2 quartz + sulfides + minor epidote; and Stage 3 laumontite, heulandite, calcite, and prehnite) that sometimes have reopened the older veins. The host basalt displays a uniformly mottled medium gray color with visible black clay pseudomorphs after olivine phenocrysts and altered plagioclase phenocrysts (light gray in the photographs).

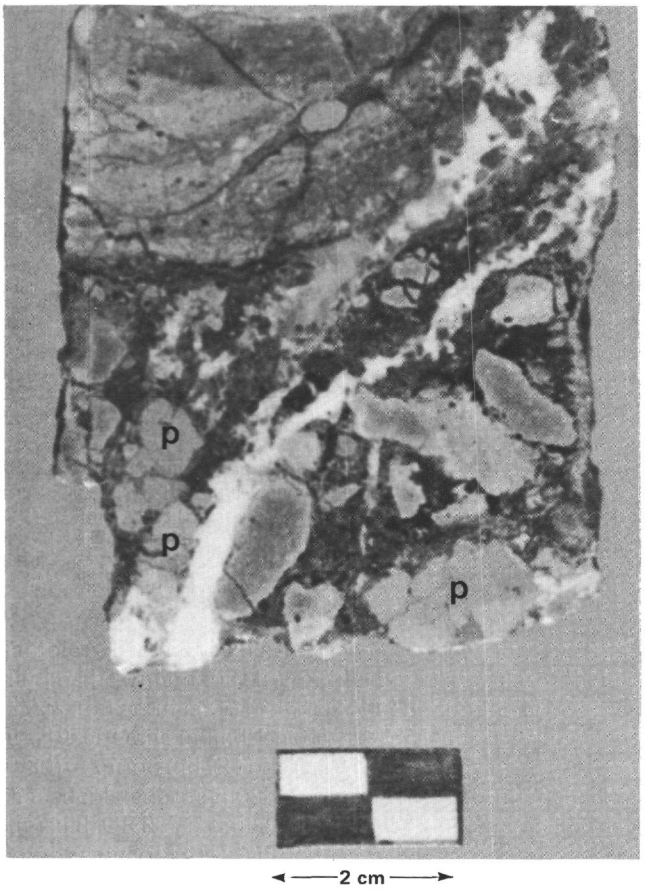

Figure 5. Sample 504B-80-2, 91–97 cm is a slab through the outer part of a fractured and metamorphosed pillow lava grading from the pillow interior (upper left corner) through the pillow rim to a pillow breccia. The breccia is made up of extensively altered pillow fragments and glass shards containing large pyrite crystal aggregates (p) up to 2 cm across. Dark green Stage 1 chlorite and chlorite-smectite mixtures form the matrix cementing the breccia and filling the cracks in the pillow lava. Rare pyrite also occurs in the clay mineral veins. Anastamosing white veins of Stage 2 quartz, pyrite, sphalerite, chalcopyrite, and galena (in decreasing order of abundance) cut across the pillow rim, the pillow fragments, and Stage 1 chloritic veins. These veins are in turn reopened and filled with and cut by Stage 3 laumontite, heulandite, calcite, and minor prehnite (white).

phenocrysts, and occasionally form networks within the pseudomorphs.

Vugs are filled with chlorite and chlorite-expandable clay mixtures and an unidentified fibrous brown subisotropic material. The fibrous brown material yields X-ray diffraction peaks of epistilbite, but microprobe analyses are high in Mg, Fe, and Mn, suggesting the presence of a clay mineral, possibly mixed with Fe-Mn oxides (Table 1, Analyses 5 and 6).

Quartz also occasionally occurs filling or lining the rims of vugs.

Plagioclase is always extensively altered or totally replaced by albite, heulandite, laumontite, and calcite in decreasing order of abundance (Plate 1, Fig. 3). A microprobe analysis of albite replacing plagioclase is given in Table 1, Analysis 8).

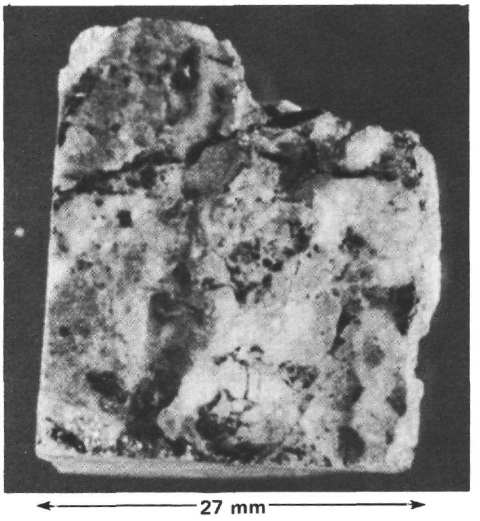

Figure 6. Sample 504B-81-1, 6–9 cm is a pillow breccia displaying a mottled light to dark greenish gray color (various grays in the photograph). It is formed by extensively altered rock fragments from pillow interiors and rims, cemented by Stage 2 milky white quartz, and cut by a clear white quartz and calcite vein up to 3 mm thick (not visible in photograph). Specks of pyrite, chalcopyrite, and sphalerite up to 1 mm in diameter are disseminated in the cement.

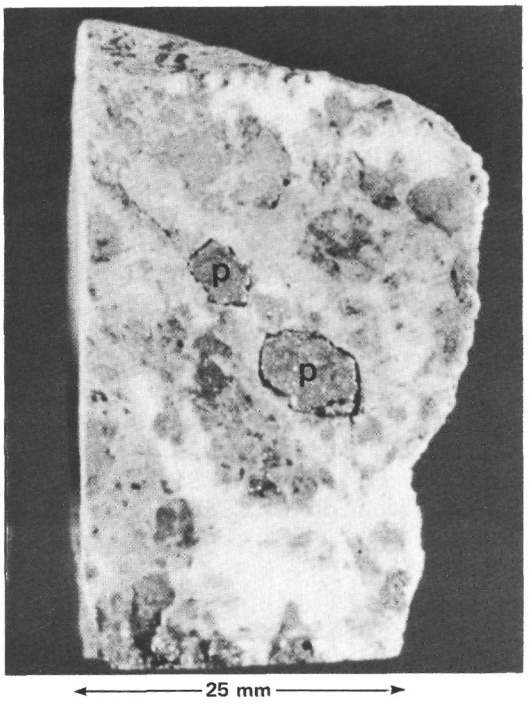

Figure 7. Sample 504B-84-2, 36–40 cm is a complex breccia exhibiting two stages of cementation. Extensively altered greenish gray rock fragments (gray in photo) are cemented by intergrown Stage 2 quartz and epidote (light gray in photo), and large pyrite crystal aggregates up to 8 mm long (p in photo). These fragments and cement are in turn broken and cemented by later Stage 3 laumontite (white in photo). Laumontite also fills the remaining pore spaces in the earlier quartz-epidote cement. Even though this sample is from 20 m below the lower part of the stockwork-like zone, it is described here because it contains large pyrite crystals that were analyzed for S isotopes along with those from the stockwork.

Table 1. Microprobe analyses of secondary minerals from Leg 83 stockwork-like zone.

Analysis	Core-Section (interval in cm)	Description	SiO_2	TiO_2	Al_2O_3	FeO^T	MnO	MgO	CaO	Na_2O	K_2O	Total
1	80-1,106–111	Stage 1 chlorite with minor expandable layers exhibiting first-order interference colors	29.00	0.04	20.43	15.12	0.78	20.06	0.27	0.14	0.09	85.93
2	80-1,106–111	Stage 1 chlorite with minor expandable layers exhibiting anomalous blue interference colors adjacent to Analysis 1	31.21	0.03	17.85	14.31	0.62	22.92	0.29	0.05	0.04	87.32
3	80-1,106–111	Stage 2 late clay mineral in vein	39.62	0.01	20.04	11.36	0.68	11.97	3.42	0.16	0.08	87.36
4	80-1, 106–111	Stage 2 late clay mineral in vein	33.84	0.02	24.72	10.67	0.61	10.83	3.14	0.34	0.20	84.42
5	80-1, 106–111	Fibrous brown material in vug	43.37	0.03	19.77	8.74	0.57	10.33	4.48	0.20	0.06	87.55
6	80-1, 106–111	Dark brown, isotropic material in vug	30.60	0.03	20.13	14.78	0.85	16.58	1.20	0.13	0.06	84.36
7	80-1, 106–111	Clay mineral replacing olivine	28.99	0.25	19.87	16.36	0.92	19.72	0.41	0.33	0.03	86.87
8	81-1, 83–86	Albite replacing plagioclase phenocryst	66.62	0.01	20.10	0.05	–	–	0.38	11.37	0.03	98.58
9	80-1, 106–111	Heulandite in vein	56.97	–	17.67	–	0.01	0.01	9.12	0.53	0.13	84.45
10	80-2, 91–97	Analcite in vein	58.77	0.01	22.91	–	0.01	0.01	0.30	11.93	0.03	93.98
11	80-2, 91–97	Laumontite replacing analcite in vein	56.87	0.02	22.53	–	–	0.02	8.84	3.25	0.05	91.58
12	80-2, 91–97	Laumontite replacing quartz in vein[a]	54.24	0.01	21.83	–	–	0.02	11.05	0.61	0.16	87.94
13	80-1, 100–111	Calcite in vein	–	–	–	–	0.59	–	50.60	–	–	51.19
14	81-1, 83–86	Actinolite reaction rim on clinopyroxene phenocryst	53.41	0.07	2.58	14.95	0.42	13.50	13.02	0.26	0.02	98.23

[a] Typical of laumontite from Leg 83 basalts (Alt et al., this volume).

Clinopyroxene is generally unaltered, but is occasionally partly cloudy due to partial oxidation indicated by dusty secondary magnetite. Actinolite sometimes occurs as reaction rims on clinopyroxene crystals and along cracks in clinopyroxene phenocrysts. Actinolite needles also project inward from the walls of clay mineral pseudomorphs after olivine phenocrysts. A microprobe analysis of actinolite replacing a clinopyroxene phenocryst is given in Table 1, Analysis 14).

Glass at pillow rims and in breccias is totally replaced by chlorite-expandable clay mixtures and sphene. Minor amounts of glass are also partly replaced by laumontite and heulandite in Sample 504B-80-2, 91–97 cm.

Pillow fragments in breccias are more extensively altered than the homogeneous (not brecciated) basalt samples. Plagioclase phenocrysts are totally replaced by albite; titanomagnetite is replaced by sphene; and the remainder of the pillow basalt fragments are extensively replaced by clay minerals, sphene, and quartz.

Veins

Cracks exhibit three basic stages of secondary mineral deposition: (1) clay minerals, (2) quartz and sulfides, and (3) zeolites and calcite (Plate 1, Figs. 1, 2). X-ray diffraction indicates that the clay minerals are chlorite, frequently with minor amounts of expandable layers (both smectite and vermiculite). The clay minerals are pale green to tan and exhibit anomalous blue to first-order interference colors. The composition of the clay minerals is slightly variable (Table 1, Analyses 1 and 2). Contents

of Fe and Al covary with Si and Mg, with the clays containing greater amounts of expandable layers also containing greater amounts of Si and Mg. The clay minerals in the stockwork-like zone are enriched in Mn relative to those in the rest of the hole (up to about 1 wt.% vs. about 0.2 wt.%, respectively; Alt et al., this volume).

Occasionally an earlier generation of quartz precedes the clay mineral formation in veins. Fine-grained quartz lines the walls of these veins, and wall rock adjacent to these veins is extensively silicified (replaced by quartz and sphene) for up to about 100 μm. Fragments of this early quartz are occasionally observed within the clay minerals filling the vein. The early quartz occurs in the same samples that contain quartz partly replacing olivine phenocrysts, and continues for about 27 m below the stockwork zone (Alt et al., this volume).

The second generation of vein minerals is characterized by the formation of quartz and sulfides. Quartz occurs as clear euhedral prismatic crystals, up to 0.7 × 2.5 mm in size, and as subhedral aggregates filling veins and cementing breccias. Breccia cements are often slightly cloudy from inclusions of clay minerals. Quartz fills reopened clay mineral veins, cuts across clay mineral veins and associated pyrite "stringers" in the wall rock, and cuts clay-mineral-cemented breccias. Reopening of clay mineral veins is indicated by the presence of fragmented clay mineral aggregates cemented by quartz in veins (Plate 1, Fig. 1), and by quartz veins that cut across and follow along clay mineral veins for short distances (Fig. 4A). Sulfides (described later) and minor epidote occur intergrown with quartz in veins. A second generation of clay minerals generally occurs intergrown with the quartz associated with sulfides (Plate 1, Fig. 1). The later clay minerals are similar in structure to the earlier clay minerals and are tan in color with anomalous blue to first-order gray interference colors. Microprobe analyses of the late clay minerals are extremely variable in composition, with high Ca contents and occasionally low totals (Table 1, Analyses 3 and 4). The clays are intimately intergrown with quartz and later zeolites, which may account for some of the compositional variability.

Epidote occurs in several samples in very small amounts as euhedral prismatic crystals, up to 15 × 150 μm, intergrown with quartz in veins.

The third stage of crack filling is characterized by the formation of zeolites. Laumontite is the most abundant zeolite in veins and occurs as coarse, platy crystals filling space between quartz crystals in veins and breccias. Laumontite also occurs in veins up to about 1 cm wide that cut across earlier veins. A typical analysis of laumontite is given in Table 1, Analysis 12. Heulandite has a similar occurrence, and although it is less abundant than laumontite, it is almost ubiquitous in small amounts, partly replacing quartz in veins (Plate 1, Fig. 3; Analysis 9, Table 1). Laumontite also occasionally replaces quartz in veins. Calcite often occurs as clear sparry crystals filling the remaining space in quartz and zeolite veins, or in monomineralic veinlets that often cut across other veins (Plate 1, Fig. 2). Calcites in the stockwork generally contain no detectable Mg, but contain up to 1 mol % Mn (Table 1, Analysis 13; Alt et al., this volume). In some cases (e.g., Samples 504B-80-1, 106–111 cm and 504B-80-2, 91–97 cm), it was found, when following along a calcite vein, that the calcite abruptly terminates against laumontite that fills the remainder of the vein, suggesting that calcite and zeolites formed simultaneously. In other cases, the relationship is not clear.

Analcite occurs in a vein of Sample 504B-80-2, 91–97 cm (Table 1, Analysis 10) and is partly replaced by Na-rich laumontite (Table 1, Analysis 11) indicating that analcite preceded laumontite. Stilbite was identified by X-ray diffraction in a vein with clay minerals, quartz, calcite, laumontite, and sulfides in Sample 504B-80-1, 30–32 cm, but was not observed in thin section so its relationship to the other minerals is not known.

Prehnite is the last mineral to form, and occurs in minor amounts as bundles or patches of radiating fibers replacing quartz and laumontite in stockwork veins.

Opaque Mineral Petrography

Preliminary microprobe analyses of stockwork sulfides are presented in Table 2.

Pyrite

Pyrite is by far the most abundant sulfide in the stockwork-like zone. Aggregates of euhedral to subhedral coarse-grained pyrite (up to 1.5 mm) are very common in the wall rock. The pyrite replaces igneous silicates, especially plagioclase, and many inclusions of silicates remain trapped in the pyrite (Plate 2, Figs. 1, 2). The pyrite aggregates frequently form millimeter-wide stringers parallel to clay veins and 4–6 mm away from them (Fig. 4B), but also occur randomly distributed in the wall rock. Veins of sphalerite fill cracks and partly replace some of the pyrite aggregates (Plate 2, Figs 2, 5).

Pyrite also occurs as fine-grained (10–20 μm) overgrowths on sphalerite grains, often developing crystal outlines (Plate 2, Figs. 3, 4), or as anhedral growths on and between grains of sphalerite (frontispiece, Fig. 4; Plate 3, Figs. 2, 3).

Large (up to a few cm) euhedral to subhedral aggregates of pyrite are fairly common in veins and breccias, where they extend into and replace surrounding wall rock (Fig. 5). These large aggregates are occasionally observed surrounding sphalerite grains.

Deeper in the hole (e.g., Cores 504B-129 and 504B-130) pyrite is also found filling narrow cracks between silicates and partly replacing the latter. This pyrite is occasionally associated with a softer, pleochroic (yellow to cream) phase displaying stronger anisotropy than chalcopyrite. This unidentified phase has been found only in minor amounts as grains up to 50 μm in diameter. In some cases, pyrite surrounds grains of magnetite (Plate 4, Fig. 6).

Magnetite

Igneous magnetite is an accessory mineral. Skeletal grains are common in the wall rock, but they are partially or totally altered to sphene and unidentified mixtures in the stockwork-like zone.

Table 2. Preliminary microprobe analyses of sulfides from the Hole 504B stockwork-like zone, Sample 504B-80-2, 13–16 cm.

	Pyrite replacing wall rock	Pyrite replacing wall rock	Pyrite in vein	Chalcopyrite	Sphalerite	Sphalerite	Galena	Galena
S	51.2	51.6	51.7	34.4	32.8	33.2	12.7	12.9
Fe	47.2	46.5	47.3	30.8	5.4	6.6	—	—
Cu	—	—	—	33.7	—	—	—	0.1
Co	—	—	—	—	—	—	—	—
Pb	—	—	—	—	—	—	83.9	84.0
Zn	—	—	—	—	60.7	60.6	0.7	—
Ni	0.4	0.2	—	—	—	—	—	—
Total	98.8	98.3	99.0	98.9	98.9	100.4	97.3	97.0

Note: Dashes indicate elements analyzed for, but not detected.

Sphalerite

Sphalerite is the second most abundant sulfide mineral, and is only observed in veins of the stockwork-like zone and in two samples from deeper in the hole (Samples 504B-94-1, 132–135 cm; 504B-97-1, 88–90 cm). Narrow veinlets (about 6 μm) are filled with sphalerite (Plate 2, Figs. 2, 5), whereas wider veins contain discontinuous coarse grains of sphalerite, mostly a few hundred microns in size, but ranging up to 2 mm in diameter (frontispiece, Figs. 1, 2, 5, 6; Plate 3, Figs. 1–3).

Sphalerite always contains abundant blebs of chalcopyrite (≤ 1 μm) that occur in three distinct patterns: (1) Chalcopyrite blebs are randomly distributed in sphalerite occurring in narrow veinlets (Plate 2, Figs. 2,5). This sphalerite is opaque in transmitted light from the abundance of chalcopyrite inclusions. (2) Chalcopyrite blebs occur in multiple concentric zones within the sphalerite grains (frontispiece, Fig. 1). (3) Chalcopyrite blebs are concentrated mainly toward the sphalerite grain boundaries (frontispiece, Figs. 2, 5; Plate 4, Figs. 1–3) or along cracks cutting across sphalerite grains (frontispiece, Figs. 2, 3).

Sphalerite exhibits various shades of gray when observed in reflected light in doubly polished sections. In the same sections observed in transmitted light, sphalerite is optically zoned, varying in color from brownish orange to yellow orange to very pale yellow or colorless (frontispiece, Figs. 1–3). Zoning is common in sphalerite in various ore deposits, with the various shades of yellow and orange because of differing iron contents. In the stockwork samples, the concentric zones of chalcopyrite inclusions tend to occur in the deeper brownish orange (Fe-rich) zones of sphalerite, whereas the yellow orange and colorless sphalerite zones are generally free of chalcopyrite. However, where chalcopyrite blebs are concentrated along sphalerite grain boundaries and cracks, the host sphalerite is frequently pale yellow (frontispiece, Fig. 2b). Cracks in sphalerite are also often healed by very pale yellow or colorless sphalerite. The colorless sphalerite always occurs as overgrowths (up to 500 μm wide), but mostly about 50 μm wide) on darker colored sphalerite, frequently with chalcopyrite blebs concentrated at the boundary between the darker and colorless sphalerite (frontispiece, Fig. 1b).

Small star-shaped inclusions of sphalerite are common in coarse granular chalcopyrite (frontispiece, Figs. 5, 6). This is a typical exsolution texture found in chalcopyrite from various ore deposits. In our samples the sides of the star-shaped inclusions are parallel to twin planes of the chalcopyrite.

Chalcopyrite

Chalcopyrite is less abundant than sphalerite, with which it is most commonly associated, although discrete grains of chalcopyrite also occur. By far the most noticeable occurrence of chalcopyrite is as fine blebs in sphalerite, both zonally distributed and along grain boundaries and cracks (see sphalerite description). When observed with high magnification the blebs are not spherical, but very often have straight sides and angular shapes.

The grain size of coarse chalcopyrite varies widely, ranging up to a maximum of 1 mm, but most grains are less than 300 μm in size. Coarse-grained chalcopyrite occasionally occurs as discrete grains, with or without star-shaped sphalerite inclusions. These grains are often found close to the more common chalcopyrite–sphalerite aggregates, both within the stockwork-like zone and deeper in the hole (Core 504B-111; Plate 4, Figs. 1, 2).

Chalcopyrite occurs in veins, most commonly in contact with coarse-grained sphalerite (frontispiece, Fig 5). These grains of chalcopyrite contain inclusions of sphalerite, some of which are star shaped (frontispiece, Fig. 6). When observed under crossed nicols, chalcopyrite grains from Cores 504B-81 and 504B-94 exhibit twins that do not extend completely across each grain.

Chalcopyrite also is commonly found as large bodies (up to 100 μm) partially or totally enclosed in sphalerite grains (frontispiece, Figs. 1a and 3). No sphalerite inclusions were observed in this chalcopyrite.

Narrow veinlets of chalcopyrite are observed in a vein of chlorite, quartz, and minor calcite and calcic zeolites, where coarse-grained sphalerite is abundant. One grain of this sphalerite is cut by a 5-μm-wide chalcopyrite veinlet with associated galena (Plate 3, Fig. 2a).

Galena

Galena is a minor component and was observed in only three samples (504B-80-2, 13–16 cm; 504B-80-2, 63–67 cm, and 504B-80-2, 91–97 cm). In Sample 504B-

80-2, 63–67 cm, galena occurs in a 5-μm chalcopyrite vein through a grain of sphalerite (Plate 3, Fig. 2a) and as a 30-μm grain attached to the outer surface of another sphalerite grain (frontispiece, Fig. 1).

GEOCHEMISTRY

Oxygen and Carbon Isotopes

Oxygen and carbon isotopic data are given in Table 3. Secondary mineral $\delta^{18}O$ values are similar to those found in minerals in hydrothermally altered basalts from dredge hauls and ophiolites (Muehlenbachs and Clayton, 1972; Heaton and Sheppard, 1977; Stakes and O'Neil, 1982; Cocker et al., 1982). Carbonate $\delta^{13}C$ values from Leg 83 basalts are lighter than those reported from other DSDP basalts (e.g., Muehlenbachs, 1977) and are similar to those from hydrothermally altered basalts in ophiolites (Cocker et al., 1982). No sulfate (anhydrite) inclusions were observed in the sulfides from Hole 504B, and no anhydrite was found at all in the stockwork zone.

Sulfur Isotopes

Pyrite samples were mechanically separated from the rock by hand picking under a binocular microscope, and were checked for purity by X-ray diffraction. Sphalerite and chalcopyrite could not be separated because the two minerals occur intergrown on a micrometer scale. The pyrite samples were dissolved in a mixture of concentrated HNO_3, concentrated HCl and Br_2 saturated water, and sulfate precipitated as $BaSO_4$ by addition of 10% $BaCl_2$ solution. The SL-277-1 standard, composed of Ag_2S, was prepared slightly differently, omitting Br_2 and precipitating with $BaNO_3$ solution to avoid Ag-halide precipitation. The $BaSO_4$ precipitates were thermally decomposed to SO_2 (Bailey and Smith, 1972) and analyzed on a Micromass 602 ratio mass spectrometer. The reproducibility of the method is approximately ± 0.15‰ (1σ). The SL-277-1 standard gave a value of +2.5‰ Cañon Diablo Troilite standard (CDT) using our laboratory standard as a reference. Previously reported values for this standard are +2.54‰ and +2.52‰ (Rees, 1978) and +2.52‰ (Halas et al., 1979/1980).

Sulfur isotope ratios ($\delta^{34}S$) measured in four hand-picked vein pyrites and one disseminated pyrite (bulk rock) sample from the stockwork zone are shown in Table 4. The values range from +3 to +5‰ CDT and are similar to but slightly heavier than those reported from hydrothermal sulfides at the East Pacific Rise, 21°N (Hekinian et al., 1980; Styrt et al., 1981).

Table 3. Isotopic data for stockwork zone samples from Hole 504B.

Core-Section (interval in cm)	Description	$\delta^{18}O$ ‰ SMOW	$\delta^{13}C$ ‰ PDB
80-1, 30–32	Calcite	+9.6	−6.1
80-1, 33–37	Bulk rock	+5.9	
80-1, 106–111	Calcite	+10.6	−5.1
	Quartz	+11.1	
	Chlorite	+1.3	
80-2, 63–67	Calcite	+13.3	−5.0
80-2, 91–97	Calcite	+14.6	−4.4
81-1, 83–87	Altered glassy pillow rim	+5.1	

Trace Elements

Splits of the sulfides analyzed for sulfur isotopes, along with two additional pyrites and one sphalerite, were analyzed for selected trace elements. X-ray diffraction indicates that the sphalerite contains trace amounts of chalcopyrite. Samples were dissolved as described previously for sulfur isotopic analyses. Trace element analyses were run on a Perkin Elmer Model 403 flameless atomic absorption spectrophotometer using standard techniques. Results are given in Table 4. The variable analytical errors in Table 4 are due to varying sample sizes.

Se and As contents are generally low, although one sample is significantly enriched in As relative to the others. Ni contents are highly variable, reaching up to greater than 1000 ppm in several samples. Copper contents tend to be higher in the stockwork samples (Cores 504B-80 and 504B-81) than in deeper samples (Table 4). The sphalerite sample is enriched in Cu relative to the pyrites because of small amounts of included chalcopyrite. Evidence exists that Se may be preferentially incorporated into chalcopyrite (Bethke and Barton, 1971), which may explain why the sphalerite sample has the highest Se content. The high As content of pyrite from Sample 504B-84-2, 36–40 cm may be due to inclusions of traces of As-bearing phases as those formed in sulfide deposits at 21°N on the East Pacific Rise (Oudin, 1983), although none have been identified yet from Leg 83 samples.

Fluid Inclusions

Freezing and heating measurements were made in a modified USGS stage similar to that described by Hollister et al. (1981). Accuracy of the heating measurements was determined to be ± 2 and ± 0.05°C for the freezing measurements using the standards recommended by MacDonald and Spooner (1981); precision of the heating measurements was ± 1°C based on repeated analyses of the same sample and standards. The samples were tested for leakage during the measurements by observing if the vapor to liquid ratio of the inclusion changed after the temperature measurements were made and by duplication of the temperature determinations.

All the fluid inclusions from Leg 83 samples are small (≤ 15 μm). Inclusions were found chiefly in quartz with lesser amounts in analcite and calcite (Table 5); no inclusions were found in sphalerite. Most of the inclusions occurred in small clusters within mineral grains or at reaction fronts of different minerals (e.g., laumontite replacing analcite; Table 5).

Filling temperatures of inclusions in quartz range from 138 to 337°C, with the maximum temperatures measured in Sample 504B-81-1, 26–30 cm. Temperatures of filling of inclusions in calcite are lower, and range from 203 to 215°C. Fracture-controlled secondary inclusions are also present in the samples. The secondary fluid inclusions also give high filling temperatures, in one case greater and the other lower than the primary inclusions in the same crystal (Table 5).

Table 4. Sulfur isotopic and trace element data for sulfides in Hole 504B stockwork-like zone. Trace element concentrations given in ppm.

Core-Section (interval in cm)	Description	$\delta^{34}S$ (‰ CDT)	Se	As	Ni	Cu	Se:S ($\times 10^5$)	As:S ($\times 10^5$)
80-1, 30-32	Vein pyrite	+3.4	10 ± 1.5	13 ± 2	1060 ± 6	214 ± 1	1.9	2.5
80-1, 33-57	Vein pyrite	+3.5	31 ± 5		530 ± 17	114 ± 2	5.8	
80-1, 33-37	Vein sphalerite		71 ± 10		590 ± 54	857 ± 7	22.0	
80-1, 34-38	Bulk rock	+2.9						
80-2, 63-67	Vein pyrite	+5.0	0 ± 3.7	25 ± 5	1680 ± 14	196 ± 2		4.8
80-2, 91-97	Vein pyrite	+3.1	13.2 ± 3		1740 ± 11	160 ± 2	2.5	
80-2, 91-97	Pyrite in hyaloclastite	+3.0	11 ± 1	13 ± 1	844 ± 4	79 ± 1	2.1	2.5
82-1, 90-96	Vein pyrite		0 ± 6		286 ± 80	79 ± 10		
84-1, 125-129	Vein pyrite		42 ± 10		935 ± 78	72 ± 10	7.9	
84-2, 36-40	Pyrite in breccia		2.6 ± 3.3	660 ± 42	321 ± 13	42.6 ± 2	0.5	125.0
Seawater[a]							0.02	0.22
Basalt[b]							17.0	100.0

[a] Quinby-Hunt and Turekian, 1983.
[b] Wedepohl, 1978. Assuming 1000 ppm S in basalt.

Table 5. Fluid inclusion geothermometry, Hole 504B.

Core-Section (interval in cm)	Sample type	Inclusion type[a]	Homogenization temperature (°C)	Filling temperature (°C)[b]	Remarks
80-1, 30-32	Calcite	P	177	215	
	Calcite	P	165	203	
	Quartz	P	244	282	
	Quartz	S	100	138	Cloudy, altered quartz
80-2, 91-97	Quartz	P	190	228	
	Quartz	P	190	228	
	Quartz	S	212	250	(Fracture controlled)
	Analcite	P	215	253	Reaction front in which laumontite is replacing analcite
	Analcite	P	215	253	
	Analcite	P	212	250	
	Analcite	P	215	253	
81-1, 26-30	Quartz	P	224	262	
	Quartz	P	300	238	
	Quartz	P	295	333	
	Quartz	P	299	337	

[a] P = primary; S = secondary.
[b] Pressure corrections applied to the homogenization temperatures are assuming a salinity of 3 wt.% equivalent NaCl, 350 bars of pressure and using Potter's (1977) data.

The paucity and small size of the fluid inclusions made freezing temperature determinations difficult. Nevertheless, three freezing temperature determinations in quartz and analcite (Sample 504B-80-2, 91-97 cm) indicate 3.5 wt.% salinites for the hydrothermal solutions, suggesting they were predominantly seawater. Similar data were obtained by Le Bel and Oudin (1982) from fluid inclusions from "black smokers" from the East Pacific Rise near 21°N.

DISCUSSION

Alteration Processes and Paragenetic Sequences

Three main stages can be reconstructed from the secondary mineral parageneses recognized in Cores 504B-80 and 504B-81, where the stockwork-like mineralizations were found: (1) formation of greenschist-facies parageneses in veins and host rocks, (2) sulfide mineralization in veins and (3) zeolite formation in veins and host rocks.

Stage 1

Stage 1 starts with minor local silicification of small rock fragments and wall rock adjacent to fissures and precipitation of fine-grained quartz along the walls of these cracks. The occasional quartz partly replacing olivine probably also formed at this time. This initial part of Stage 1 is more commonly observed below the stockwork zone down to 955 m BSF (i.e., 27 m below the bottom of the stockwork). In the voids between pillow fragments and in fissures the local early quartz is followed by chlorite and minor pyrite, whereas albite, chlorite and chlorite-expandable clay mixtures, actinolite, sphene, and pyrite partly replace the primary phases of the host rocks. The pyrite in the host rocks formed "stringers" parallel to clay mineral veins during this stage. This first stage of secondary mineral precipitation appears to have sealed up the first network of cracks and cemented the pillow fragments into a breccia. As a consequence, the permeability that must have been very large initially in

this portion of Hole 504B was probably greatly reduced. The minerals formed during the first stage belong to the greenschist facies of regional metamorphism. However, the basalts from the stockwork-like zone did not reach equilibrium under the greenschist facies (or any other facies) conditions. The $\delta^{18}O$ value of 1.3‰ for a chlorite sample from a Stage 1 vein suggests that it formed from a fluid very near seawater composition and at temperatures of 200–250°C (Hattori et al., 1980) The formation of Mg-rich clay minerals during Stage 1 suggests that fluids were Mg-bearing, but some of the Mg in solution could have been released from basalts, which in some cases have lost Mg (Alt and Emmermann, this volume). The Mn enrichments of the clay minerals in the stockwork-zone basalts suggest the presence of evolved fluids, perhaps partially reacted seawater that could be enriched in Mn and Fe, but still contain Mg (Seyfried and Mottl, 1982). These fluids were also probably enriched in silica, causing the replacement of olivine by quartz. Water/rock mass ratios for the stockwork zone calculated on the basis of Mg uptake by the metabasalts are generally very low (Alt and Emmermann, this volume).

Stage 2

During Stage 2, veins of quartz and Fe, Zn, Cu, and Pb sulfides formed, with minor chlorite and chlorite-expandable clay mixtures and local traces of epidote. These sulfide-bearing veins cut across the Stage 1 veins and frequently reopened them. The abundance of polymetallic sulfides visible to the unaided eye distinguishes Cores 504B-80 and 504B-81 from the rest of the Leg 83 cores and led us to call this zone of Hole 504B a stockwork-like mineralization.

Two generations of sphalerite, at least three of chalcopyrite, and one each of galena and pyrite formed during Stage 2. The first sulfides to appear during Stage 2 are chalcopyrite and sphalerite. Sphalerite continued to crystallize after chalcopyrite ceased to grow, as indicated by the relatively large (hundreds of μm) chalcopyrite bodies included within sphalerite grains in veins (frontispiece, Fig. 1A). Fluctuations in the temperature and/or composition of the hydrothermal solutions occurred during sphalerite growth, as shown by the zonal distribution of chalcopyrite blebs and color zoning in sphalerite. The zonal distribution of chalcopyrite blebs probably resulted from recurring periods of epitaxial growth of chalcopyrite during continued sphalerite growth. Experimental evidence indicates that the solubility of Cu in sphalerites crystallizing at less than about 650°C is insignificant (Hutchinson and Scott, 1981). Since Leg 83 sphalerites probably did not form at temperatures greater than 350°C (see following discussion), the possibility of fine chalcopyrite blebs in sphalerite originating by exsolution can be discarded. On the other hand, the presence of sphalerite stars in chalcopyrite grains can be explained by exsolution of zinc sulfide from the chalcopyrite host. Even though the solubility of ZnS in chalcopyrite is relatively low at 250–350°C, exsolution of small amounts of sphalerite from chalcopyrite in ores formed at these temperatures is common (J. Craig, personal communication, 1983).

The color zoning of sphalerites generally parallel the outlines of the crystals and may be due to variations in FeS content of the grains (Browne and Lovering, 1973), MnS content, or other factors under study (Barton, personal communications, 1983). This variation of Fe content may be the result of fluctuations in sulfur fugacity and/or temperature of the hydrothermal solutions (Barton and Toulmin, 1966).The abundant pyrite and the absence of pyrrhotite in the stockwork-like zone samples indicate that sulfur fugacities were above the pyrite/pyrrhotite boundary.

Reaction of late Cu-bearing hydrothermal solutions with sphalerite resulted in the formation of chalcopyrite "disease" (the fine blebs of chalcopyrite) along cracks and exposed surfaces, in some cases forming the lath- or rodlike chalcopyrite inclusions along crystallographic direction in sphalerite. Barton (1978) described similar occurrences of chalcopyrite disease in sphalerites from the Furutobe Mine, Japan, and Creede, Colorado. Barton (personal communication, 1983) suggested that the process seems to be iron-conservative and that zinc is removed to accommodate copper introduced as chalcopyrite without volume change. Chalcopyrite disease cuts across the color zonation and epitaxial inclusions of chalcopyrite in Leg 83 sphalerites, indicating that it formed relatively late in the history of sphalerite growth. In some cases intergranular spaces between grains of sphalerite and cracks in sphalerite remain open even though solutions penetrated to form chalcopyrite disease, but in other cases the cracks were sealed by late, colorless sphalerite, indicating that chalcopyrite disease preceded the formation of colorless sphalerite. Chalcopyrite disease does not affect the late, colorless sphalerite overgrowths. Chalcopyrite disease may be responsible in part for the abundant inclusions of fine chalcopyrite blebs near the outer edges of sphalerite grains. However, at least some of this chalcopyrite is also due to inclusions of epitaxial growths, as indicated by the multiple concentric bands observed at some sphalerite grains (frontispiece, Fig. 1). Microprobe analyses will be carried out so as better to understand the pattern.

Chalcopyrite disease generally occurs within about 10–20 μm of the sphalerite grain margins and cracks. However, small sphalerite grains (i.e., less than 10–40 μm) and sphalerite in narrow veinlets could have been completely affected by chalcopyrite disease, resulting in the random distributions of chalcopyrite blebs throughout small sphalerite grains and in narrow veinlets (Plate 2, Fig. 5). Reheating and/or recrystallization could also result in coalescing of chalcopyrite inclusions (Stanton, 1972; Barton, 1978) and may have caused the overall and random distributions and/or the larger sizes of chalcopyrite blebs in some sphalerite grains. In at least one sample, a late-generation chalcopyrite fills a crack in sphalerite, with the host sphalerite displaying chalcopyrite disease along the crack (Sample 504B-80-2, 63–67 cm; Plate 3, Fig. 2A). The late chalcopyrite in the crack and the chalcopyrite disease in the host sphalerite reach up to the edge of the sphalerite; a late, colorless sphalerite overgrowth occurs on the sphalerite grain, but not on the late chalcopyrite in the crack. We interpret this to in-

dicate that the colorless sphalerite overgrowth formed after the late chalcopyrite filling the crack. Nucleation effects may have inhibited colorless sphalerite from growing on the chalcopyrite in the crack. A similar effect may explain frontispiece, Fig. 1A.

Galena occurs in the late chalcopyrite filling the crack in sphalerite in Sample 504B-80-2, 63–67 cm, indicating that galena formed relatively late in the sulfide mineral sequence.

The last sulfide mineral to form is a second generation of pyrite, occurring as fine overgrowths on both colored and colorless sphalerite and as large euhdral crystals in veins and replacing wall rock adjacent to veins. The cessation of Cu, Zn, and Pb sulfide deposition may reflect a decrease in temperature of hydrothermal solutions and/or a decrease in the respective metal contents of solutions. Evidence (see Stage 3) indicates that temperatures following sulfide deposition were lower, but absolute timing of Stage 3 relative to sulfide deposition is unknown.

Although only pyrites were analyzed for $\delta^{34}S$, both Stage 1 (pyrite disseminated in wall rock stringers; bulk rock Sample 504B-80-1, 34–48 cm) and Stage 2 pyrites (from veins) are represented. There is no significant difference in the sulfur isotopic composition of pyrites from the different stages; the Stage 1 pyrite $\delta^{34}S$ value falls within the range of the Stage 2 pyrites (Table 4). The $\delta^{34}S$ values of the stockwork pyrites are significantly greater than those of primary sulfides in tholeiitic basalts, which range from -3 to $+1.5$‰ (Schneider, 1970; Kanehira et al., 1973). In both the pyrites from Hole 504B and the East Pacific Rise "black smokers" at 21°N, the increase in $\delta^{34}S$ probably results from the reduction of seawater sulfate circulating through basalts at elevated temperatures.

Unfortunately, the sulfur isotope data alone do not constrain the proportions of basaltic and seawater sulfate sulfur in the sulfides. As discussed by Styrt et al. (1981), such calculations are very sensitive to the fraction of sulfate reduced in the hydrothermal solutions, an unknown quantity. Without constraining this parameter, we can say only that the contribution of reduced seawater sulfate lies roughly between 15 and 80% of the stockwork sulfur.

In some cases deposition of sulfides and silicates may have occurred simultaneously during Stage 2; for example, in the cases where quartz occurs as isolated idiomorphic crystals with sphalerite and chalcopyrite in veins filled with later zeolites and where quartz and sulfides entirely fill reopened Stage 1 chlorite veins. Vermicular chlorite and trace amounts of epidote occur intergrown with quartz in the latter case. However, in some cases clay minerals fill cracks in sphalerite grains, indicating that the silicates formed after sphalerite. Also, quartz and late clay minerals often fill spaces between sphalerite grains, indicating that silicates continue to crystallize after sphalerite formation ceased.

According to primary fluid inclusion data, temperatures of formation of quartz range from 203 to 338°C (Table 5). The range in filling temperatures within single samples indicates fluctuations in temperature and multiple generations of quartz deposition. Oxygen isotope and fluid inclusion measurements have not all been made on exactly the same samples However, if it is assumed that the quartz from Core 504B-80 that was analyzed for $\delta^{18}O$ (Sample 504B-80-1, 106–111 cm) formed at temperatures similar to those measured from fluid inclusion data in the same core (228–282°C; Table 4), then the fluid in equilibrium with the measured quartz $\delta^{18}O$ value (11.1‰; Table 3) would have had a $\delta^{18}O$ value of $+1$ to $+4$‰ (Clayton et al., 1972). Oxygen isotopic data on a quartz-epidote pair from Core 90 in Hole 504B (67 m below the stockwork) suggest temperatures of formation of up to 380°C and possible formation from ^{18}O-enriched fluids (Alt et al., this volume). Freezing temperature measurements of fluid inclusions in quartz indicate that salinities of Stage 2 hydrothermal fluids were close to that of seawater.

Stage 2 does not appear to have altered the metabasalts resulting from the first alteration stage, since the minerals found in the mineralized veins have not generally been observed in the host metabasalts. The only exception would be the late pyrite that occasionally extends from the veins into the wall rock, which it locally replaces. Deeper in the hole (Cores 504B-94 and 504B-111) not only pyrite but also sphalerite and chalcopyrite occasionally replace the wall rock of mineralized veins.

Stage 3

Stage 3 is essentially represented by the crystallization of zeolites and calcite. Rare analcite and stilbite occur locally in veins and preceded the other zeolites as indicated by the replacement of analcite by laumontite. Analcite may have formed at temperatures lower than 200°C, since it occurs in contact with quartz in Leg 83 basalts, and at temperatures higher than 200°C (500 bars P_{H_2O}; analcite should react with quartz to form albite (Liou, 1971a). Stilbite breaks down to form laumontite and quartz at temperatures greater than 150°C (500 bars P_{H_2O}) Liou, 1971c). Both experimental reactions are reversible and hence represent equilibrium reactions. In contrast, the veins of Cores 504B-80 and 504B-81 record the effects of nonequilibrium reactions in an open hydrothermal system, suggesting that the experimental data may not be applicable.

Laumontite and calcite are the two most abundant minerals crystallizing during Stage 3. They fill up new cracks, fill spaces left open in Stage 2 veins, and replace plagioclase in the host rock. Fluid inclusions in analcite close to the replacement front where analcite is being replaced by laumontite indicate that this reaction occurred at 250°C. This temperature is higher than that at which laumontite reversibly dehydrates to form wairakite (231°C at 500 bars P_{H_2O}; Liou, 1971b). This observation indicates either that wairakite initially replaced analcite at 250°C and was later hydrated to form laumontite as the system cooled below 237°C or that laumontite represents a metastable replacement of analcite at 250°C. The overall disequilibrium nature of the parageneses observed in Hole 504B and the lack of any wairakite relics support the latter alternative. On the other hand, adjacent quartz and analcite in Sample 504B-80-2, 91–97 cm

show no signs of reaction with each other, and both phases have been extensively replaced by laumontite. This supports the suggestion that analcite formed at lower temperatures (possibly less than 200°C), where reaction rates would be slower.

Heulandite probably formed at the same time as laumontite in the Leg 83 stockwork zone samples. In regionally metamorphosed basic rocks heulandite is generally observed in lower-grade rocks (i.e., shallower rocks, altered at lower pressure and temperature), whereas laumontite occurs in higher-grade rocks (Winkler, 1979). However, the temperature-stability fields of the two minerals overlap, with heulandite stable at higher silica activities (Boles and Coombs, 1977).

Calcite precipitating from normal seawater at 25°C contains about 8 mole % Mg (Mucci and Morse, 1983) and the Mg content of calcite increases with temperature (Fuchtbauer and Hardie, 1976). No Mg was detected by microprobe or by X-ray diffraction in calcite from the stockwork-like veins, in spite of fluid inclusion data that indicate that they formed at temperatures of up to 215°C. The calcites thus probably formed from Mg-depleted solutions. The negative carbonate $\delta^{13}C$ values suggest a contribution of mantle carbon (−7‰; Pineau et al., 1976) by basaltic magma.

Calcite in Sample 504B-80-1, 30–32 cm has a $\delta^{18}O$ value of +9.6‰ and a fluid inclusion filling temperature of 203–215°C (Tables 2 and 4). Assuming a temperature of formation of 203°C for this calcite, the fluid in equilibrium with calcite with the measured $\delta^{18}O$ value would have had a $\delta^{18}O$ value af about +1‰ (O'Neil et al., 1969). The calculated temperature of formation of the other two calcites in Table 3 range from 135 to 189°C assuming equilibrium with a fluid with a $\delta^{18}O$ value of 0‰, or from 145 to 210°C assuming equilibrium with a fluid of +1‰ (O'Neil et al., 1969). In some samples (e.g., Samples 504B-80-1, 106–111 cm and 504B-80-2, 91–97 cm), calcite appears to have formed simultaneously with the calcic zeolites suggesting that the latter formed over a range of temperatures. In other cases the relationship between calcite and zeolite is not clear, suggesting that calcite possibly formed later and at a lower temperature than the zeolite. An alternative explanation would have calcite re-equilibrate at a lower temperature after having crystallized with the zeolites.

The formation of all Stage 3 minerals would have been favored by more evolved ("rock-dominated") Mg-depleted hydrothermal solutions with higher pH compared to those of the preceding two stages. Fluid inclusion data indicate that the salinity of the hydrothermal fluids did not deviate significantly from seawater values.

Comparison of the Hole 504B Sulfides to Seafloor Sulfide Deposits

The most obvious difference between the Hole 504B sulfide mineralizations and the seafloor sulfide deposits at 21°N on the East Pacific Rise is that the former occur in veins in altered basalts and thus must have formed below the seafloor, although the depth of formation is unknown. Other major differences are the presence of abundant quartz, the predominance of pyrite among the sulfides, the absence of wurtzite, and the lack of many minor and accessory sulfides (e.g., pyrrhotite, etc.) in the Hole 504B samples (Haymon and Kastner, 1981; Oudin, 1983). Based on thermodynamic calculations and the absence of quartz in the 21°N deposits, Bischoff (1980) suggested that those deposits formed by adiabatic expansion of hydrothermal fluids and predicted that deposits formed by cooling or mixing of similar hydrothermal fluids with seawater should contain abundant quartz. The association of sulfide mineralization with abundant quartz in veins of Leg 83 basalts appears to be consistent with this prediction. The absence of pyrrhotite and wurtzite in the Hole 504B mineralizations can be explained in different ways. It was suggested (Haymon and Kastner, 1981) that rapid precipitation led to metastable formation of pyrrhotite and wurtzite in "black smoker" deposits at 21°N under conditions at which pyrite and sphalerite should have been stable. Slower crystallization rates in fissures of crustal rocks in Hole 504B would hence explain the absence of wurtzite and pyrrhotite. Furthermore, wurtzite and pyrrhotite are replaced by pyrite and sphalerite, respectively, during evolution of the seafloor deposits at lower temperatures (Haymon and Kastner, 1981; Oudin, 1983) and thus might be expected to be absent from older deposits such as those in Hole 504B.

Alternatively, sulfur fugacity was too high for pyrrhotite to form, and hence the Zn/S ratio was also too low for wurtzite to crystallize; according to Scott and Barnes (1972) wurtzite and sphalerite are not true polymorphs of ZnS, but the former crystallizes when the Zn + Fe/S > 1 and the latter when Zn + Fe/S ≤ 1.

Heat Source and Timing of Sulfide Mineralizations

The mineralizations of the stockwork-like zone of Hole 504B are clearly hydrothermal in origin, as is indicated by the abundance of hydrated secondary minerals both as veins and alteration products of the host rocks and the frequency of fluid inclusions in hydrated and anhydrous secondary minerals. These minerals formed at temperatures ranging from 140 to 340°C. Had the mineralizations formed by burial metamorphism at the 636 m sub-basement depth, one could calculate thermal gradients ranging from 280 to 570°C/km. If the mineralizations had formed at shallower depths, or even the surface of the old seafloor, the thermal gradients would have been higher. Let us consider now the possible heat sources for such hydrothermal processes in the upper oceanic crust.

Magmatic activity at or very close to the spreading center during or shortly after the emplacement of the basalts in which the mineralizations occur is the most likely heat source. Hot springs debouch onto the seafloor of the East Pacific Rise spreading axis at temperatures of 320 and 360°C, at 13 and 21°N, respectively, and are presently depositing transition metal sulfides similar to those observed in the stockwork-like zone of Hole 504B (Michard et al., 1983; Rise Project Group, 1980). Other hot springs have been found at oceanic spreading centers with temperatures much lower than 100°C (e.g., Galapagos Spreading Center, Corliss et al., 1979). How-

ever, the temperatures at depth inferred from the geochemistry of these hydrothermal solutions are of the same order as those of the East Pacific Rise at 21 and 13°N (Edmond et al., 1979). All of these high-temperature hot springs are restricted to a narrow zone, a few hundreds of meters wide, at the spreading axis.

Intraplate magmatism is unlikely to be a source of hydrothermal activity since no evidence for such activity has been observed between the Costa Rica Rift and Site 504 (Langseth et al., 1983). With the exception of seamounts 50 km off the East Pacific Rise at 21°N (Lonsdale et al., 1982), no evidence exists to support off-axis or ridge-flank high-temperature hydrothermal activity either on or below the seafloor. In the hydrothermal mounds located 20 km south of the Galapagos Spreading Center the maximum measured temperature is 15°C, and from the solution geochemistry it can be inferred that the temperature of the basalt–seawater reaction at depth is less than 100°C (Maris and Bender, 1980). Chemical gradients in sediment pore waters near Site 504, 200 km south of the Costa Rica Rift, indicate interaction of seawater with underlying basalt (Mottl et al., 1983). However, the equilibrium temperature at the bottom of the 1350-m-deep Hole 504B is only 165°C, indicating relatively low-temperature reactions in crust reheated during a conductive thermal regime (Langseth et al., 1983).

Because of the very large permeability of upper oceanic crust pillow basalts, high-temperature hydrothermal activities on or near the seafloor are probably short lived. Away from the shallowest portion of the magma chamber, both along the strike of the spreading axis (e.g., see fig. 10 in Mottl, 1983) and transversely to it, the 360°C isotherm progressively but relatively rapidly sinks below the seafloor. The same temperature distribution should be observed through time in a "dying" magma chamber, that is, a chamber not replenished by magma. Unfortunately the size and shape of spreading axis magma chambers are virtually unknown. In summary, high-temperature hydrothermal solutions resulting from basalt–seawater reactions appear to occur relatively briefly on the seafloor only at or very near the spreading axis during the lifetime of magma chambers.

Although the question of the absolute timing of alteration and sulfide mineralizations relative to the age of crustal formation remains unresolved, the restriction of high-temperature hydrothermal activity close to the spreading axis suggests that the Hole 504B sulfide mineralizations occurred within this zone. The repeated reopening of filled cracks and the opening of new cracks indicate alteration in a tectonically active area, possibly in the zone of extension close to the spreading axis, which supports this interpretation. Since the host rocks for the stockwork-like mineralizations are pillow basalts and breccias that must have been exposed at one time on the seafloor, the sulfide mineralization thus may have been emplaced very near the seafloor close to the axis of spreading.

Alternatively, mineralizations may have formed slightly off-axis, but not more than a couple of kilometers from the axis, in the high-temperature upwelling limb of a convection cell. In this case the sulfides could have formed at greater depths under a basalt pile up to 635 m thick (the present thickness of the overlying basalt section).

CONCLUSIONS

The relatively young (5.9 m.y old) basalts of the Hole 504B stockwork-like zone contain complex mineral parageneses and structural features indicating a similarly complex alteration history. Alteration of the basalts occurred in three general stages (summarized in Fig. 8).

1. Minor local deposition of quartz along walls of veins and silicification of adjacent wall rock was followed by formation of chlorite and chlorite-expandable clay mixtures, and minor pyrite veins, and albite, sphene, chlorite, actinolite, and pyrite replacing primary phases in the host rocks. Pyrite "stringers" also formed in wall

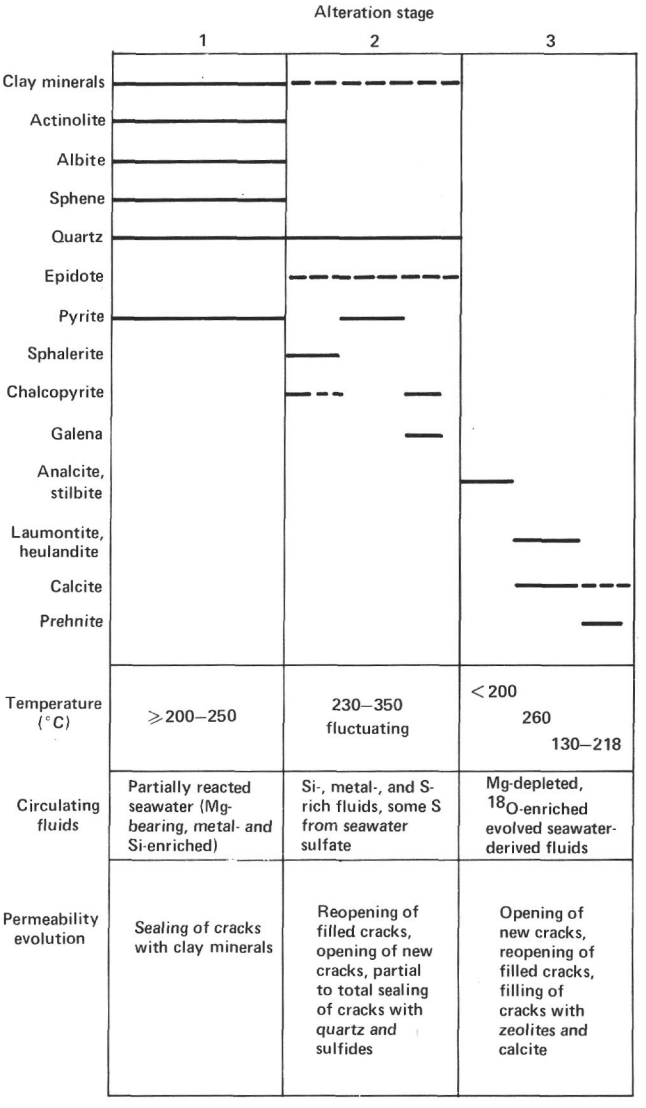

Figure 8. Summary diagram showing stages of alteration and mineral deposition with chemical conditions for each stage.

rock adjacent to chlorite veins. During the first stage circulating fluids were probably partially reacted seawater, and temperatures were at least 200–250°C.

2. Cracks filled during the first stage were reopened, along with new cracks. These were filled with quartz, clay minerals (chlorite and chlorite-expandable clay mixtures), traces of epidote, and pyrite, sphalerite, chalcopyrite, and galena. The mineralizing solutions were relatively evolved metal- and Si-rich hydrothermal fluids. Pyrite $\delta^{34}S$ values range from +2.9 to +5.0‰ and indicate that some of the sulfide sulfur was derived from reduction of seawater sulfate. Temperatures of mineralization ranged from 230 to 340°C, with fluctuations in temperature and composition of fluids recorded in a complex sequence of sulfide mineral deposition—chalcopyrite, ± Fe-rich sphalerite, chalcopyrite disease, Fe-poor sphalerite, chalcopyrite, galena, and pyrite.

3. The last stage is characterized by zeolite and low Mg-calcite formation in the remaining space in earlier cracks, in reopened and newly opened cracks, and replacing plagioclase in the host rocks. Analcite and stilbite were the first zeolites to form in veins, possibly at temperatures below 200°C. Temperatures fluctuated during this third stage, as is indicated by the replacement of analcite and quartz by laumontite at 250°C and the formation of calcite at temperatures ranging from about 135 to 220°C. During the last stage fluids were depleted in Mg and enriched in Ca and probably ^{18}O relative to seawater; they contained a mantle carbon component. This sequence can be interpreted as being due to the effects of a relatively long-term evolution of the hydrothermal system upon which there were superimposed shorter term fluctuations in solution temperature and composition. The latter were a response to changes in the permeability of the formation that were related to multiple fracturing caused by the tectonic activity of the moving plate.

The mineralizations successively formed in the pillow basalts and breccias on or close to the seafloor relatively shortly after the lavas were emplaced at or near the spreading axis of the Costa Rica Rift. A cooling magma chamber probably located below the spreading axis, acted as the heat source that drove the hydrothermal system.

It is astonishing to find such a complex mineralization history that includes three generations of fissures each followed by a secondary mineral parageneses in a young crust and that is the result of a relatively simple hydrothermal system (i.e., tholeiites reacting with seawater). Clearly these complexities must be initially responsible for some of the even more complex textures and mineralogies observed in much older kuroko-type massive sulfides in Japan and metamorphized massive sulfides such as those found in Canada (see review by Franklin et al., 1981).

ACKNOWLEDGMENTS

We thank D. Price and A. Castellanos for their assistance and P. B. Barton, P. M. Bethke, and S. D. Scott for helpful discussions. This research was supported by NSF Grant OCG 81-17698 to J. Honnorez. Eric Saltzman was supported by Petroleum Research Grant No. 1348AC2. The paper was reviewed by P. B. Barton and R. M. Haymon. Contribution from Rosenstiel School of Marine and Atmospheric Science, University of Miami.

REFERENCES

Anderson, R., Honnorez, J., et al., 1982. DSDP Hole 504B, the first reference section over 1 km through layer 2 of the oceanic crust. *Nature*, 300:589–594.

Bailey, S. A., and Smith, J. W., 1972. Improved method for the preparation of sulfur dioxide barium sulfate for isotope ratio studies. *Anal. Chem.* 44:1542–1543.

Barton, P. B., 1978. Some ore textures in involving sphalerite from Furutobe Mine, Akita Prefecture, Japan. *Min. Geol.*, 28:293–300.

Barton, P. B., and Toulmin, P., 1966. Phase relations involving sphalerite in the system Fe-Zn-S. *Econ. Geol.*, 61:815–849.

Bethke, P. M., and Barton, P. B., Jr., 1971. Distribution of some minor elements between coexisting sulfide minerals. *Econ. Geol.*, 66: 140–163.

Bischoff, J. L., 1980. Geothermal system at 21°N East Pacific Rise: Physical limits on geothermal fluid and role of adiabatic expansion. *Science,* 207:1465–1469.

Boles J. R., and Coombs, D. S., 1977. Zeolite facies alteration of sandstones in the southland syncline, New Zealand. *Am. J. Sci.*, 277:982–1012.

Bonatti, E., Honnorez-Guerstein, B. M., and Honnorez, J., 1976. Copper iron sulfide mineralizations from the equatorial Mid-Atlantic Ridge. *Econ. Geol.*, 71:1515–1525.

Browne, P. R. L., and Lovering, J. F., 1973. Composition of sphalerites from the Broadlands geothermal field and their significance to sphalerite geothermometry and geobarometry. *Econ. Geol.*, 68: 381–387.

Clayton, R. N., O'Neil, J. R., and Mayeda, T. K., 1972. Oxygen isotope exchange between quartz and water. *J. Geophys. Res.*, 77: 3057–3067.

Cocker, J. C., Griffin, B. J., and Muehlenbachs, K., 1982. Oxygen and carbon isotope evidence for seawater-hydrothermal alteration of the Macquarie Island ophiolite. *Earth Planet. Sci. Lett.*, 61: 112–122.

Corliss, J. B., Dymond, J., Gordon, L. I., Edmond, J. M., von Herzen, R. P., Ballard, R. D., Green K., Williams, D., Brainbridge, A., Crane, K., and Van Andel. T. H., 1979. Submarine thermal springs on the Galapagos Rift. *Science*, 203:1073–1083.

Edmond, J. M., Measures, C., McDuff, R. E., Chan, L. J., Collier, R., Grant, B., Gordon, L. I., and Corliss, J. B., 1979. Ridge Crest hydrothermal activity and the balances of the major and minor elements in the ocean: the Galapagos data. *Earth Planet. Sci. Lett.*, 46:1–18.

Franklin, J. M., Sangster, D. M., and Lydon, J. W., 1981. Volcanic-associated massive sulfide deposits. *Econ. Geol. 75th Anniv. Vol.*, 485–628.

Fuchtbauer, H., and Hardie, L. A., 1976. Experimentally determined homogeneous distribution coefficients for precipitated magnesian calcites: application to marine carbonate cements. *Geol. Soc. Am. Ann. Mtg., Abstr. with progr.*, 8:877. (Abstract)

Gray, M., McAfee, R., Jr., and Wolf, C. L., (Eds.), 1974. *Glossary of Geology:* Washington, D.C. (Am. Geol. Inst.).

Halas, S., Lis, J., Szaran, J., Trenbaczowski, A., 1979/1980. A comparison of sulfur isotope standards used in different laboratories. *Ann. Univ. Mariae Curie-Sklodowska, Sec. AAA*, 34–35(5):37–43.

Hattori, K., Urabe, T., and Muehlenbachs, K., 1980. Anhydrite bodies of marine hydrothermal origin at Kuroko. *Third Int. Symp. on Water-Rock Interaction Proc.*, Edmonton, Canada, pp. 89–90.

Haymon, R. M., and Kastner, M., 1981. Hot springs deposits on the East Pacific Rise at 21°N: preliminary description and genesis. *Earth. Planet. Sci. Lett.*, 53:363–381.

Heaton, T. H. E., and Sheppard, S.M.F., 1977. Hydrogen and oxygen isotope evidence for sea-water-hydrothermal alteration and ore deposition, Troodos Complex, Cyprus. *Volcanic Processes in Ore Genesis:* London (London Inst. Mining and Metallurgy and Geological Society), pp. 42–47.

Hekinian, R., Fevrier, M., Bischoff, J. L., Picot, P., and Shanks, W. C., 1980. Sulfide deposits from the East Pacific Rise near 21°N. *Science*, 207:1433–1444.

Hollister, L. S., Crawford, M. L., Roedder, E., Burruss, R. C., Spooner, E. T. C. and Touret, J., 1981. Practical aspects of microthermometry. *In* Hollister, L. S., and Crawford, M. L., (Eds.), *Short*

Course in Fluid Inclusions: Applications to Petrology: Calgary (Mineral. Assoc. Canada), pp. 278–301.

Honnorez, J., Laverne, C., Hubberten, H., Emmermann, R., and Muehlenbachs, K., 1983. Alteration processes in Layer 2 basalts from Deep Sea Drilling Project Hole 504B, Costa Rica Rift. *In* Cann, J. R., Langseth, M. G., Honnorez, J., Von Herzen, R. P., White, S. M., et al., *Init. Repts. DSDP*, 69: Washington (U.S. Govt. Printing Office), 509–546.

Humphris, S. E., and Thompson, G., 1978. Hydrothermal alteration of oceanic basalts by seawater. *Geochim. Cosmochim. Acta*, 43: 107–125.

Hutchinson, M. N., and Scott, S. D., 1981. Sphalerite geobarometry in the Cu-Fe-Zn-S system. *Econ. Geol.*, 76:143–153.

Kanehira, K., Yui, S., Sakai, H., and Sasaki, A., 1973. Sulfide globules and sulfur isotope ratios in the abyssal tholeiite from the Mid-Atlantic Ridge near 30°N latitude. *Geochem. J.*, 89–96.

Langseth, M. G., Cann, J. R., Natland, J. H., and Hobart, M., 1983. Geothermal phenomena at the Costa Rica Rift: Background and objectives for drilling at Deep Sea Drilling Project Sites 501, 504, and 505. *In* Cann, J. R., Langseth, M. G., Honnorez, J., Von Herzen, R. P., White, S. M. et al., *Init. Repts. DSDP*, 69: Washington (U.S. Govt. Printing Office), 5–30.

Le Bel, L. and Oudin, E., 1982. Fluid inclusions studies of deep-sea hydrothermal sulfide deposits on the East Pacific Rise near 21°N. *Chem. Geol.*, 37:129–136.

Liou, J. G., 1971a. Analcime equilibria. *Lithos*, 4:389–402.

_____, 1971b. P-T stabilities of laumontite, wairakite, lawsonite, and related minerals in the system $CaAl_2Si_2O_8$-SiO_2-H_2O. *J. Petrol.*, 12:370–411.

_____, 1971c. Stilbite-laumontite equilibria. *Contrib. Mineral. Petrol.*, 31:171–177.

Lonsdale. F., Batiza, R., and Simkin, T., 1982. Metallogenesis at seamounts on the East Pacific Rise. *Mar. Tech. Soc. J.*, 16:54–61.

MacDonald, A. J., and Spooner, E.T.C. 1981. Calibration of a Linkam TH 600 programmable heating-cooling stage for microthermometric examination of fluid inclusions. *Econ. Geol.*, 76:1248–1258.

Maris, C., and Bender, M., 1980. Pore water chemistry of the Galapagos mounds hydrothermal field. *EOS*, 61(46):995. (Abstract).

Michard, A., Albarède, F., Michard, G., Minster, J. F., and Charlou, J. L., 1983. Rare-earth elements and uranium in high temperature solutions from East Pacific Rise hydrothermal vent field (13°N). *Nature*, 303:795–797.

Mottl, M. J., 1983. Metabasalts, axial hot springs and the structure of hydrothermal systems at mid-ocean-ridges. *Geol. Soc. Am. Bull.*, 94: 161–180.

Mottl, M. J., Lawrence, J. R., and Keigwin, L, D., 1983. Elemental and stable-isotope composition of pore waters and carbonate sediments from Deep Sea Drilling Project Sites 501/504 and 505.*In* Cann, J. R., Langseth, M. G., Honnorez, J., Von Herzen, R. P., White, S. M., et al., *Init. Repts. DSDP*, 69: Washington (U.S. Govt. Printing Office) 461–474.

Mucci, A., and Morse. J. W., 1983. The incorporation of Mg and Sr into calcite overgrowths: Influences of growth rate and solution composition. *Geochim. Cosmochim. Acta*, 47:217–233.

Muehlenbachs, K., 1977. Oxygen isotope geochemistry of rocks from DSDP Leg. 37. *Can. J. Earth Sci.*, 14(4–2):771–776.

Muehlenbachs, K., and Clayton, R. N., 1972. Oxygen isotope studies of fresh and weathered submarine basalts. *Can. J. Earth Sci.*, 9: 172–184.

O'Neil, J. R., Clayton, R. N., and Mayeda, T. K., 1969. Oxygen isotope fractionation in divalent metal carbonates. *J. Chem. Phys.*, 51:5547–5558.

Oudin, E., 1983. Hydrothermal sulfide deposits on the East Pacific Rise (21°N). Part I: Descriptive mineralogy. *Mar. Mining*, 4:39–72.

Oudin, E., Picot, P., and Pouit, G., 1981. Comparison of sulfide deposits from the East Pacific Rise and Cyprus. *Nature*, 291:404–407.

Pineau, F. M., Javoy, M., Bottinga, Y., 1976. $^{13}C/^{12}C$ ratios of rocks and inclusions in popping rocks of the Mid-Atlantic Ridge and their bearing on the problem of isotope composition of deep seated carbon. *Earth. Planet. Sci. Lett.*, 29:413–421.

Potter, R. W., 1977. Pressure corrections for fluid inclusion homogenization temperatures based on the volumetric properties of the systems NaCl-H_2O. *USGS J. Res.*, 5:603–607.

Quinby-Hunt, M. S., and Turekian, K. K., 1983. Distribution of elements in seawater. *EOS, Trans. Am. Geophys. Union.*, 64:130–131.

Rees, C. E., 1978. Sulfur isotope measurements using SO_2 and SF_6. *Geochim. Cosmochim. Acta*, 42:383–389.

Rise Project Group, 1980. East Pacific Rise: Hot springs and geophysical experiments. *Science*, 207:1421–1432.

Schneider, A., 1970. The sulfur isotopic composition of basaltic rocks. *Contrib. Mineral. Petrol.*, 25:95–124.

Scott, S. D., and Barnes, H. L., 1972. Sphalerite-wurtzite equilibria and stoichiometry. *Geochim. Cosmochim. Acta.*, 36:1275.

Seyfried, W. E., and Mottl, M. J., 1982. Hydrothermal alteration of basalt by seawater under seawater-dominated conditions. *Geochim. Cosmochim. Acta*, 46:985–1002.

Stakes, D. S., and O'Neil, J. R., 1982. Mineralogy and stable isotope geochemistry of hydrothermally altered oceanic rocks. *Earth Planet. Sci. Lett.*, 57:285–304.

Stanton, R. L., 1972. *Ore Petrology:* New York (McGraw-Hill).

Styrt, M. M., Brackmann, A. J., Holland, H. D., Clark, B, C., Pisutha-Arnond, U., Elridge. C. S., and Ohmoto, H., 1981. The mineralogy and the isotopic composition of sulfur in hydrothermal sulfide/sulfate deposits on the East Pacific Rise, 21°N latitude. *Earth Planet. Sci. Lett.*, 53:382–390.

Wedepohl, K. H., (Ed.) 1978. *Handbook of Geochemistry, II-3:* New York, (Springer-Verlag).

Winkler, H. G. F., 1979. *Petrogenesis at Metamorphic Rocks:* New York, (Springer-Verlag).

Date of Initial Receipt: 8 January 1983
Date of Acceptance: 15 December 1983

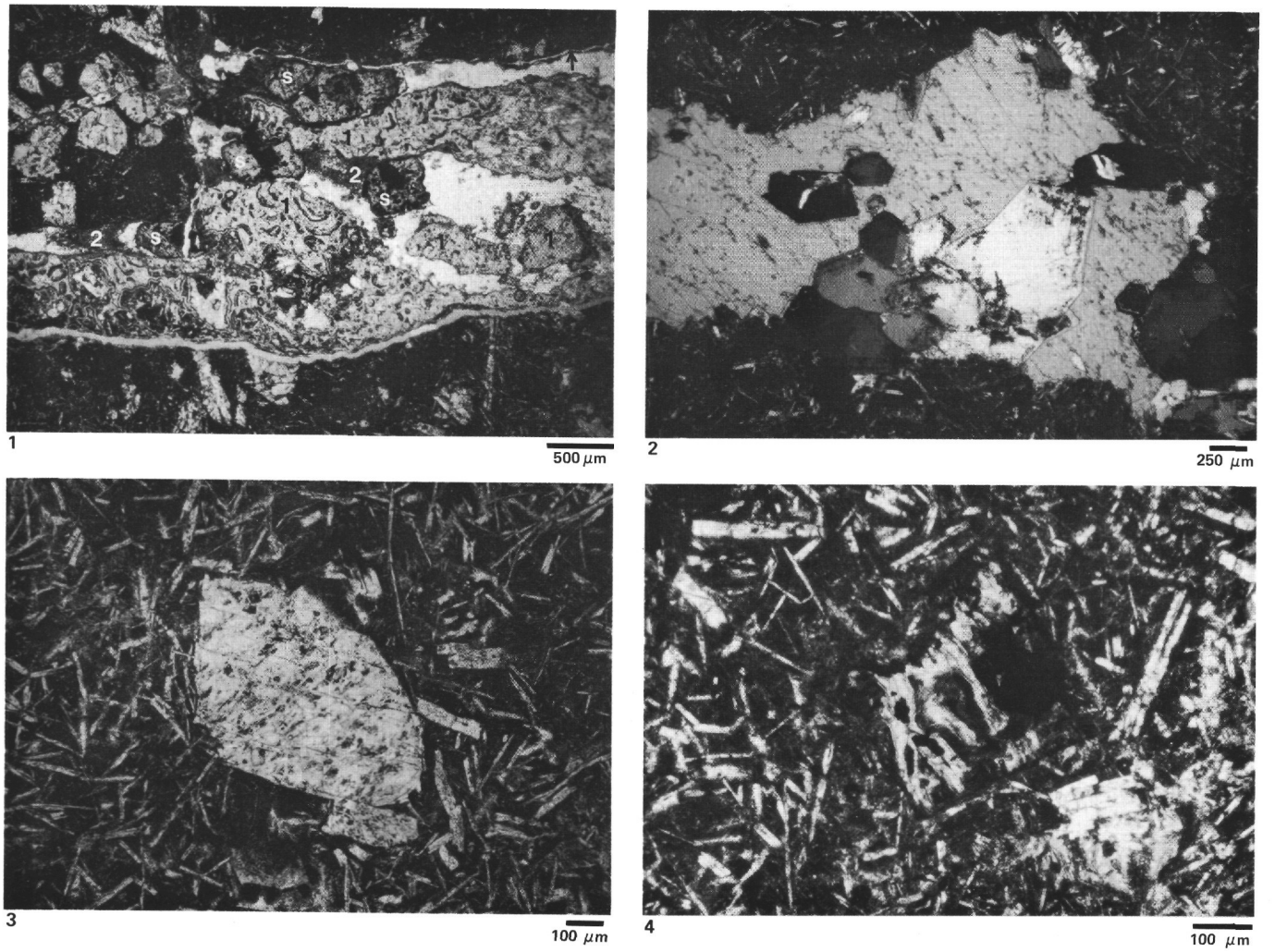

Plate 1. Transmitted light photomicrographs of secondary silicate minerals. **1.** Stage 1 chlorite vein (1) reopened and filled with sphalerite (s), chalcopyrite (black), quartz (white), and Stage 2 late clay mineral (2). Note Stage 3 Ca-zeolite veinlet (arrow, upper right) at top. The crack parallel to the bottom of the vein is filled with glue (white) where sample was glued together. Plane polarized light, Sample 504B-80-1, 106–111 cm. **2.** Euhedral quartz crystals partly replaced by heulandite in vein. Replacement is often concentrated just within the edges of the quartz. Late calcite (gray) fills space between quartz crystals. Plane polarized light, Sample 504B-80-1, 106–111 cm. **3.** Extensively albitized plagioclase phenocryst. Plane polarized light, Sample 504B-80-1, 106–111 cm. **4.** Olivine phenocryst replaced by chlorite with minor expandable layers and pyrite (black). Plane polarized light. Sample 504B-80-1, 106–111 cm.

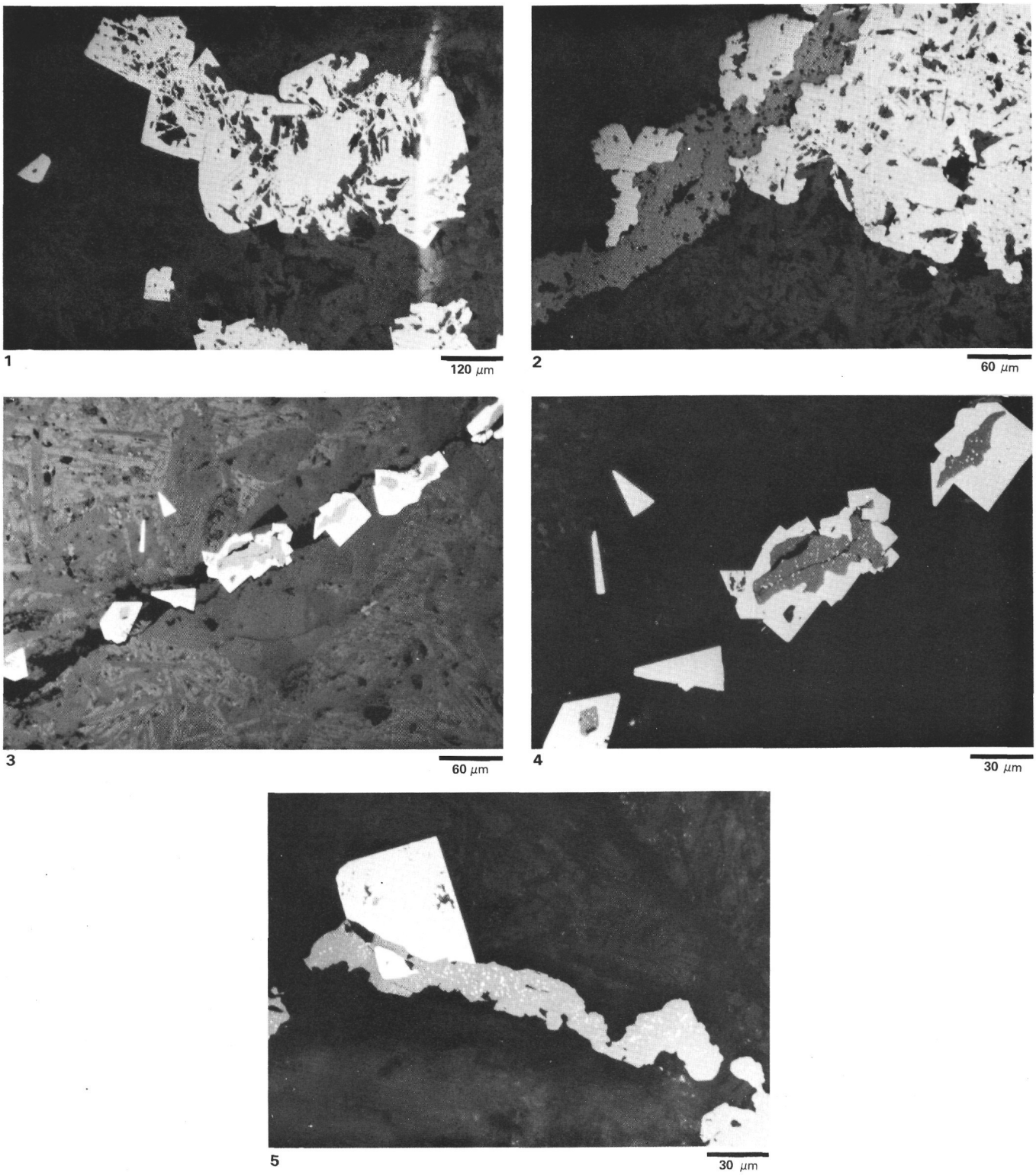

Plate 2. Reflected light photomicrographs of stockwork-like zone sulfides. **1.** Aggregate of euhedral grains of Stage 1 pyrite (white) replacing wall rock (Sample 504B-80-1, 34–38 cm). **2.** Vein of Stage 2 sphalerite (gray) containing chalcopyrite blebs cutting through and partly replacing (?) and aggregate of Stage 1 pyrite (white) (Sample 504B-80-1, 34–38 cm). **3.** Sphalerite (light gray) with chalcopyrite blebs (see **4**) is aligned along a fissure and overgrown by well-crystallized pyrite (white) (Sample 504B-80-1, 106–111 cm). **4.** Detail of 3. **5.** Vein of Stage 2 sphalerite (gray), with randomly distributed chalcopyrite blebs, cutting through a euhedral crystal of Stage 1 pyrite (white) (Sample 504B-80-1, 34–38 cm).

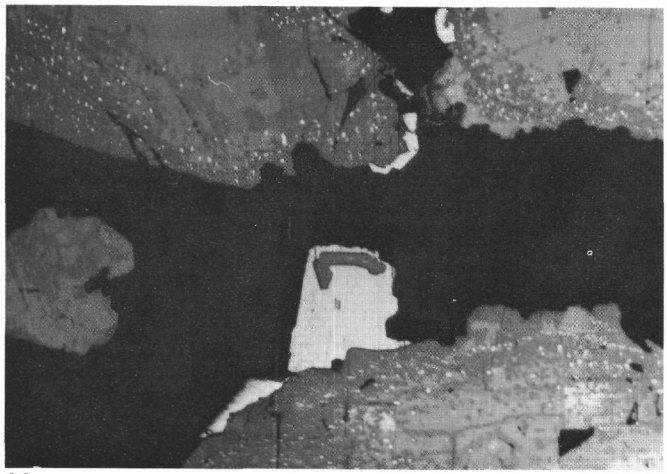

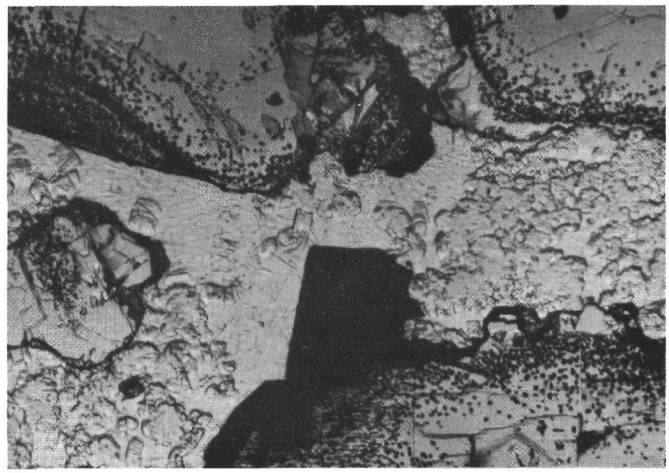

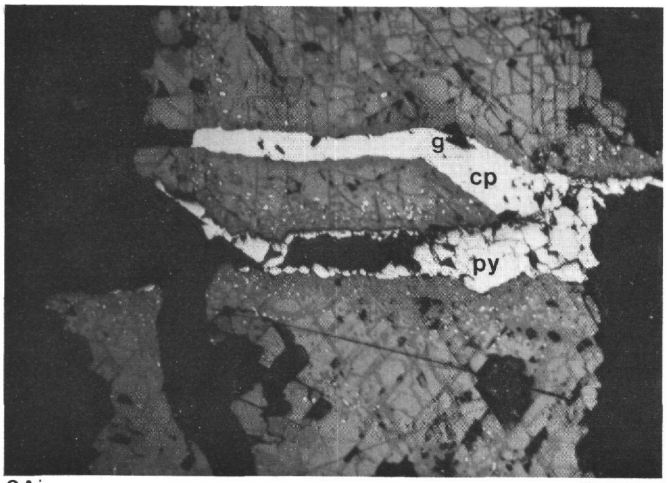

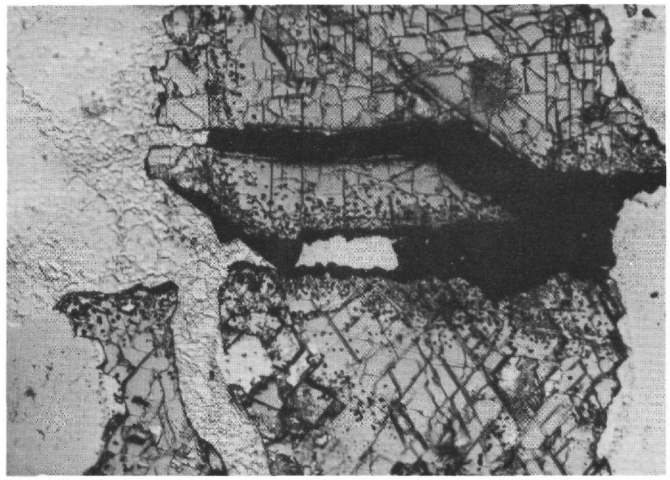

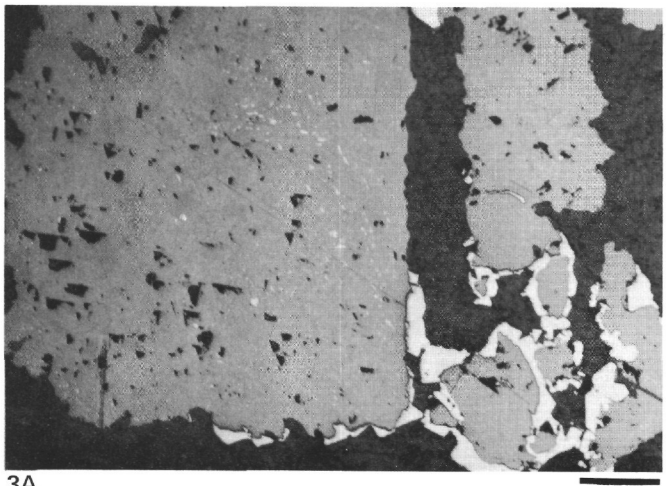

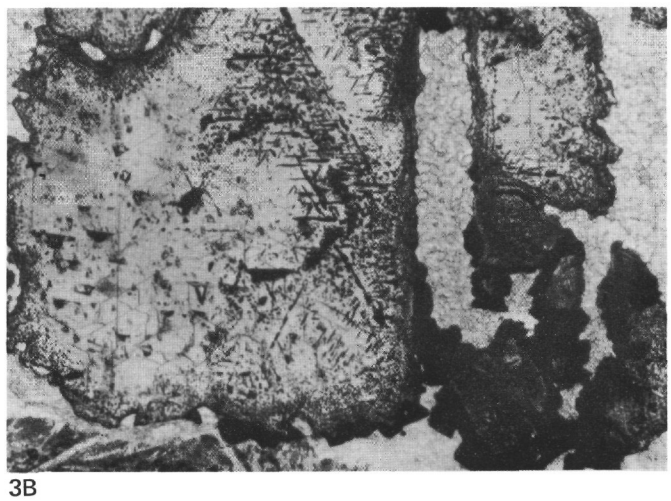

Plate 3. Photomicrographs of stockwork-like zone sulfides. Doubly polished thin sections; reflected light (a), transmitted light (b). **1A.** Grains of sphalerite (gray shades) with chalcopyrite blebs at the grain boundaries; galena (white, rectangular section) with an inclusion of sphalerite; fine-grained pyrite (white) overgrowth on sphalerite grains (Sample 504B-80-2, 63–67 cm). **1B.** Notice alignment of opaque chalcopyrite inclusions in sphalerite adjacent to galena. **2A.** Two grains of sphalerite with well-developed (110) cleavages, and chalcopyrite blebs mainly along grain boundaries. A chalcopyrite (cp) vein cutting across the sphalerite grain contains a patch of galena (g). Fine-grained pyrite (py) fills space between the sphalerite grains (Sample 504B-80-2, 63–67 cm). **2B.** Notice overgrowth of colorless sphalerite (left side of upper grain) except on chalcopyrite vein (Sample 504B-80-2, 63–67 cm). **3A.** Chalcopyrite (white) blebs and rodlike bodies included in sphalerite (medium gray). Fine-grained pyrite (white) overgrowth on sphalerite grains (Sample 504B-80-2, 63–67 cm). **3B.** Notice crystallographic orientation of chalcopyrite inclusions in sphalerite and marginal concentration of chalcopyrite blebs.

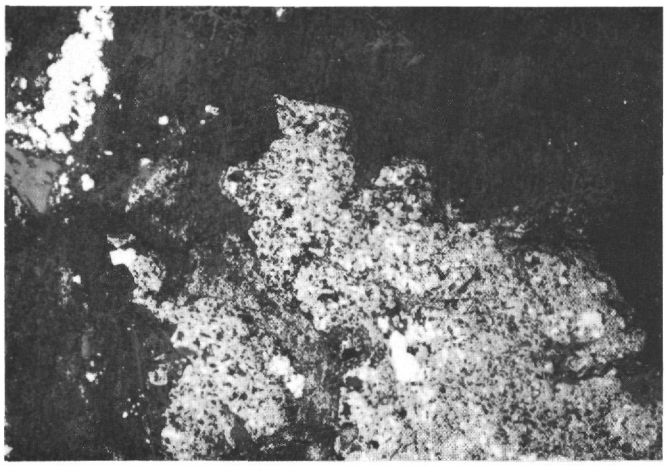

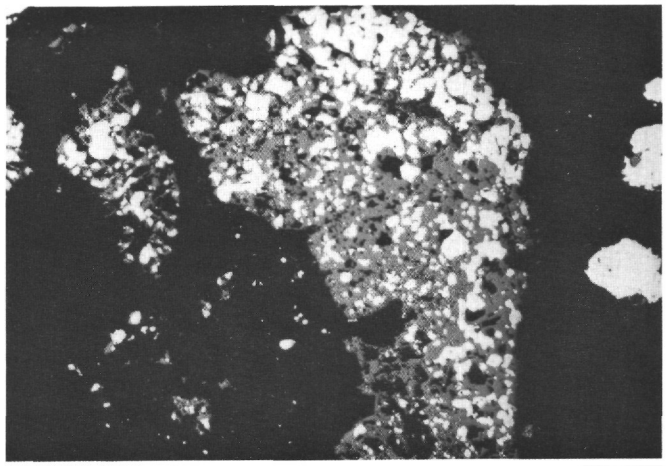

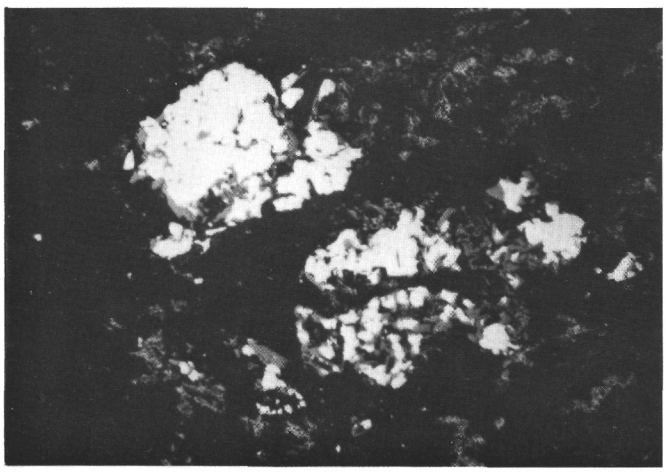

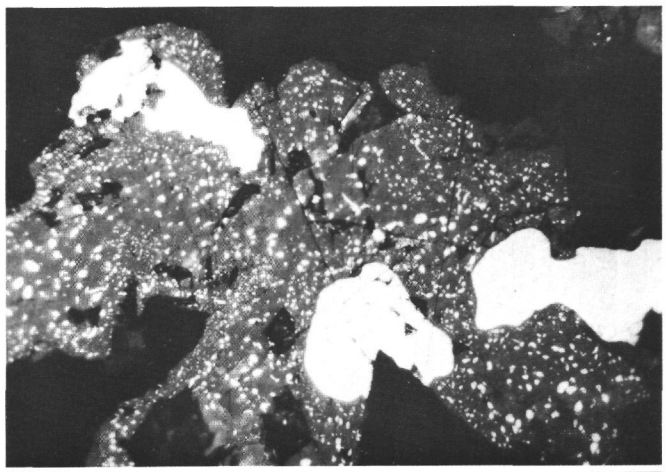

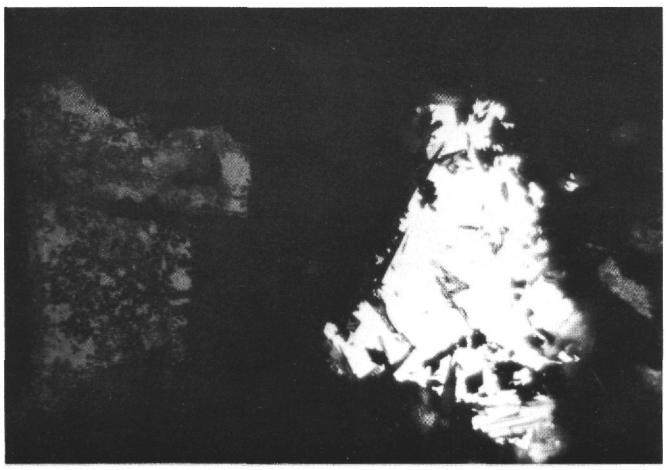

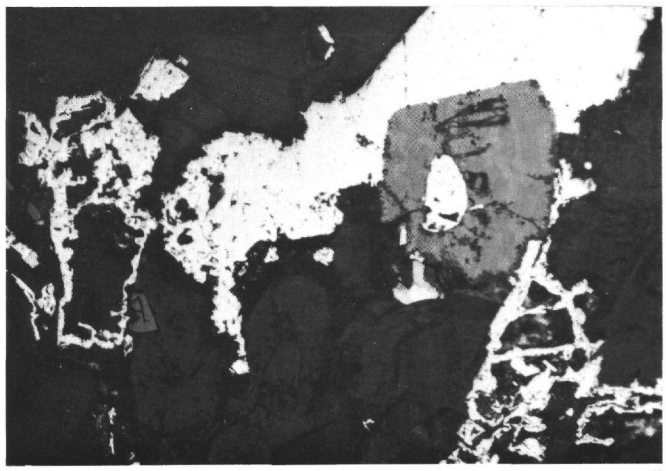

Plate 4. Reflected light photomicrographs of sulfides in samples from Hole 504B below the stockwork-like zone. **1.** Sphalerite (gray) intergrown with chalcopyrite (white) in a clay vein (dark background), and isolated grains of chalcopyrite (white) (Sample 504B-111-1, 104–107 cm). **2.** Chalcopyrite (white) intergrown with sphalerite (gray) and isolated grains of chalcopyrite (same vein as **1**). **3.** Chalcopyrite (white) associated with sphalerite (gray) (same vein as **1**). **4.** Sphalerite (gray) with large bodies of chalcopyrite (white) and smaller chalcopyrite blebs randomly distributed; very fine blebs are concentrated toward the grain boundaries (Sample 504B-97-1, 88–90 cm). **5.** Chalcopyrite (white) intergrowth with silicates, and a grain of magnetite (left, medium gray) highly altered to sphene and an unidentified fine-grained product (Sample 504B-129-1, 33–35 cm). **6.** Grain of magnetite (medium gray), slightly altered along the edge and cracks, is partly surrounded by pyrite (white). Pyrite fills cracks and replaces silicates and contains several inclusions of (?) cubanite (Sample 504B-130-2, 43–44 cm).